CDF/EXOTIC/7383
Version 2.0
May 19, 2005

A Search for Universal Extra Dimensions in the Multi-Lepton Decay Channel at the Tevatron

Chun Lin, Colin Gay, Michael Schmidt
Marcel Stanitzki, Steve Nahn, Andrew Martin, Greg Feild
Yale University

Abstract

In the Univeral Extra Dimension (UED) scenario, pair production of the first Kaluza-Klein (KK) excitation of standard particles at the Tevatron are expected to undergo cascade decays into their zero mode counterparts (standard particles) and the lightest KK particle (LKP). The LKP is the first KK excited photon, and it is stable and thus will escape the detector resulting in a missing energy signature. The signature of the UED scenario would be multiple standard leptons, jets and missing energy. We present the result from an analysis of a multi-lepton search using CDF Run IB 87.5 pb^{-1} SUSY dilepton data. We set an upper limit of total KK production cross section $\sigma_{tot} < 7.9$ pb at 95% confidence level, converting to an extra dimension radius limit of 280 GeV.

1 Introduction

The Standard Model (SM) of elementary particles has been very successful in describing the strong and electroweak interactions under the gauge group $SU(3)_C \times SU(2)_L \times U(1)_Y$. Almost all existing experimental results are consistent with the SM. There are, however, some open questions in the SM which lead us to the assumption that there must be a theory beyond the SM. One possible extension to the SM is the Universal Extra Dimensions (UED) scenario [1]. The UED scenario is an extension of the SM in which all particles live in a $(4+n)$-dimensional space. All of the SM fields propagate into extra compact dimensions of size $R \sim \text{TeV}^{-1}$.

In the UED scenario, momentum conservation in the extra dimensions leads to Kaluza-Klein (KK) number conservation at tree level. Except for zero mode mass contributions, at each level all KK particles have the same masses given by n/R. KK number conservation is violated by loop corrections and localized terms at the orbifold boundaries. However a KK parity remains conserved and leads to the existence of a stable lightest KK particle (LKP). Due to radiative corrections KK masses are shifted from their tree level values. All higher level KK particles undergo cascade decays to the LKP by emitting soft SM particles. The LKP cannot be detected directly because it interacts with normal matter very weakly, but has a mass about R^{-1}, thus resulting in large missing energy.

The current experimental bounds allow KK particles in the UED scenario to be as light as a few hundred GeV [1]. Such light KK states may be produced at the Tevatron with center of mass energies of 1.8 TeV.

The outline of this note is as follows. In the next section we review the relevant theory and the Minimal Universal Extra Dimensions (MUED) scenario. We describe the data sample selection in Section 3 and the background to our analysis in Section 4. In Section 5 we review the Monte Carlo simulations. We review the selection criteria for the analysis in Section 6 and give the results in Section 7. Discussions of radiative corrections, lepton identification requirements, signal and background Monte Carlo, $b\bar{b}/c\bar{c}$ background scale factor and charged multiplicity are included in the appendices.

2 Theoretical Framework of the UED Scenario

The Standard Model is a successful theory describing elementary particles and their interactions. There is very little experimental evidence for any physics beyond the Standard Model.

There are, however, some unanswered questions about the Standard Model. For example, why are there three generations of quarks and leptons? Does the Higgs boson exist or is it only a mechanism to explain electroweak symmetry breaking and the masses of quarks and leptons? Why can't the Standard Model incorporate gravity for energies approaching the Planck scale?

All of these facts lead us to the assumption that there must be a theory beyond the Standard Model. Many have been proposed, such as technicolor, supersymmetry (SUSY), and extra dimensions. Each of these models solves some of the above problems, but up to now there is no experimental evidence for any of these models.

In this chapter, we briefly describe theory of extra spacetime dimensions with localized fields, then discuss the UED scenario with the simplest case - the Minimal Universal Extra Dimensions (MUED) scenario, followed by a discussion of the collider phenomenology of the MUED scenario.

2.1 Theory of Extra Spacetime Dimensions

The world of everyday experience has three spatial dimensions. Einstein's theory of special relativity treats time t as a fourth dimension, together with the space coordinates they are collectively denoted x^μ.

Einstein's theory of general relativity states that physical laws should be the same to all observers. A gravitational field with two indices, $g_{\mu\nu}(x)$, which also has the geometrical interpretation of a metric tensor, was introduced. In a four-dimensional spacetime, the infinitesimal distance between two points ds is:

$$ds^2 = g_{\mu\nu}(x)dx^\mu dx^\nu \tag{1}$$

In 1919, Theodor Kaluza[2] unified Maxwell's electromagnetism with gravity by applying Einstein's general theory of relativity to a five-dimensional spacetime manifold. The postulated fifth coordinate together with the first four coordinates are denoted collectively x^M. In a five-dimensional spacetime, the line element becomes:

$$d\hat{s}^2 = \hat{g}_{MN}(x)dx^M dx^N \tag{2}$$

where

$$\hat{g}_{MN} = \begin{pmatrix} g_{\mu\nu} + \kappa^2\phi^2 A_\mu A_\nu & \kappa\phi^2 A_\mu \\ \kappa\phi^2 A_\nu & \phi^2 \end{pmatrix} \tag{3}$$

$g_{\mu\nu}$ describes Einstein's gravitational field, A_μ describes Maxwell's electromagnetic field, ϕ is a scalar field and κ is a constant ($\kappa \equiv 4\sqrt{\pi G}$, where G is gravitational constant in four dimensions); $g_{\mu\nu}$, A_μ, and ϕ transform respectively as a tensor, a vector and a scalar under four-dimensional general coordinate transformations.

Kaluza also assumed that all derivatives with respect to the fifth coordinate vanish ("cylinder condition") so that physics depends on the first four coordinates, to explain why no fifth dimension had been observed in nature.

In 1926 Oskar Klein [3] applied Kaluza's theory to quantum theory. He showed that Kaluza's cylinder condition would arise naturally if the fifth coordinate was a lengthlike one and had two properties: (1) a circular topology (S^1); and (2) a small ("compactified"[1]) scale. The space topology is then the product of a four-dimensional space and a circle: $R^4 \times S^1$, and we can envisage such topology as a tiny circle at each point in four-dimensional spacetime.

Under property (1) any physical field $f(x, y)$ (where $x = (x^0, x^1, x^2, x^3)$ denotes coordinates on R^4, and $y = x^4$ denotes the coordinate on S^1) becomes periodic, as $f(x, y) = f(x, y + 2\pi R)$, where R is the radius (scale parameter) of the fifth dimension. Therefore all the fields can be expanded in Fourier series along S^1 and we set $0 \leq \frac{y}{R} \leq 2\pi$:

$$g_{\mu\nu}(x, y) = \sum_{n\in\mathbb{Z}} \mathrm{e}^{in\frac{y}{R}} g^{(n)}_{\mu\nu}(x) \; , \tag{4}$$

$$A_\mu(x, y) = \sum_{n\in\mathbb{Z}} \mathrm{e}^{in\frac{y}{R}} A^{(n)}_{\mu}(x) \; , \tag{5}$$

$$\phi(x, y) = \sum_{n\in\mathbb{Z}} \mathrm{e}^{in\frac{y}{R}} \phi^{(n)}(x) \; , \tag{6}$$

The superscript $^{(n)}$ refers to the nth Fourier mode.

Similar to a quantum particle in a box, the momentum in the y dimension is quantized in units of $1/R$. This builds a Kaluza-Klein (KK) tower of states, with the individual KK excitations being labelled by mode numbers, n. Under property (2), if R is small enough, momentum in the y dimension of even the $n = 1$ modes will be too large to be detected

[1] A compact dimension is curled up on itself and the radius is very small. Anything moving along this dimension's direction would return to its starting point almost instantaneously. The dimension is very small (Planck scale) in Kaluza-Klein theory, so it cannot be observed by conventional methods. Recent models of large extra dimensions with radius of order 1 TeV^{-1} could be observed at the Tevatron or the LHC.

experimentally. Hence only the $n = 0$ modes, which are independent of y, will be observable. Thus the low energy (e.g. TeV scale) physics is effectively four-dimensional.

2.2 The Minimal Universal Extra Dimensions (MUED) Scenario

In the extra dimensions theory described in section 2.1, our observed 3-dimensional space is a 3-brane ("wall"), and this 3-brane is embedded in a higher D-dimensional spacetime ("bulk"), where $D = 3 + 1 + \delta$, with $\delta = 1$ for the extra one spatial dimension which is orthogonal to our 3-brane. The Standard Model fields are confined to the wall, while the gravitational field propagates throughout the bulk.

In the Universal Extra Dimensions (UED) scenario [1] however, all of the Standard Model fields are allowed to propagate in the bulk. For simplicity, we consider the UED scenario which has all of the SM fields propagating in one extra dimension compactified on a S^1/Z_2 orbifold, where Z_2 is the reflection symmetry $y \to -y$.

Throughout this article, we use the following notations, adapted from Ref. [9]: upper case letters denote $SU(2)$ doublets; lower case letters denote $SU(2)$ singlets; subscript $_n$ denotes the $n-th$ KK mode; subscript $_L$ denotes left-handedness; subscript $_R$ denotes right-handedness, e.g. Q_1 denotes $n = 1$ mode $SU(2)$-doublet quarks, q_1 denotes $n = 1$ mode $SU(2)$-singlet quarks.

The tree-level mass of the n-th KK mode satisfies:

$$m_n^2 = m_0^2 + \frac{n^2}{R^2}, \tag{7}$$

where R is the radius of the compact dimension, m_0 is the zero mode mass (Standard Model mass) and n is an integer which corresponds to the quantized momentum p_5 in the compact dimension and becomes a quantum number (KK number) under a $U(1)$ symmetry in the 4D description. Ignoring branes and orbifold fixed points, KK number is a good quantum number and is conserved in all interactions and decays. Except for zero mode mass contributions, without radiative corrections, at each level all KK modes would be degenerate in mass, with masses given by n/R, as shown in Fig. 1. The Feynman rules for the KK modes are derived in Ref. [4, 5].

The Standard Model 4D chirality is achieved by compactifing the extra dimension on a S^1/Z_2 orbifold, namely the following boundary conditions [2]:

$$\psi(x, y) = \psi(x, y + 2\pi R)\ ,\ \psi(x, y) = -\gamma^5\psi(x, -y)\ , \tag{8}$$

[2] An equivalent presentation is to treat the 5th dimension as an interval from 0 to πR. The boundary conditions at the ends of the interval are such that the odd fields vanish, and the even fields derivative along the extra dimension vanish. Here ψ describes a fermion field.

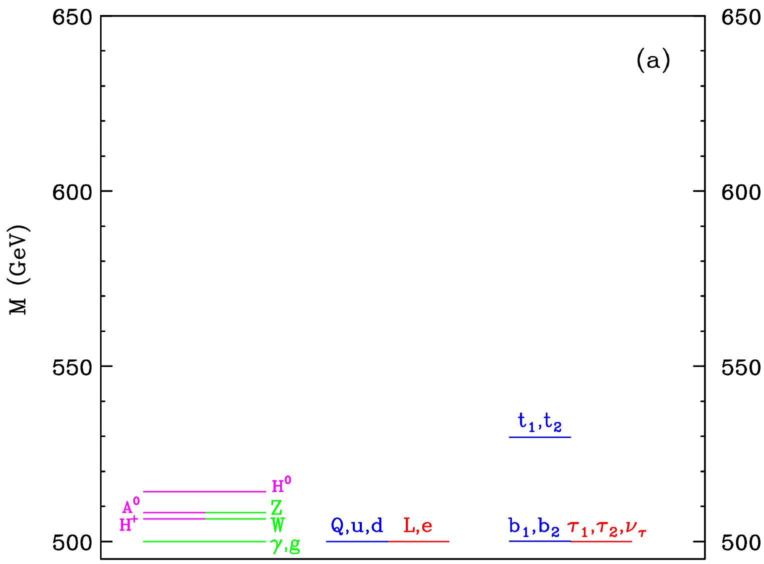

Figure 1: The mass spectrum of the $n = 1$ modes at tree level for $R^{-1} = 500$ GeV, $\Lambda R = 20$ and $m_h = 120$ GeV. Ref. [6]

which implies that there is a left-handed Z_2 even field ψ_+, and a right-handed Z_2 odd field ψ_-:

$$\psi_+(x,y) = \sum_{n=0}^{\infty} \psi_+^{(n)}(x) \cos(ny/R) \ , \ \psi_-(x,y) = \sum_{n=1}^{\infty} \psi_-^{(n)}(x) \sin(ny/R) \tag{9}$$

Note that Z_2 odd field does not have zero modes, thus we project out the zero mode fermions with the wrong chiralities and obtain the Standard Model 4D chiral fermions out of the zero modes of the 5D KK fields.

The orbifold fixed points break translational symmetry in the fifth dimension, therefore momentum in the y direction (KK number) is no longer conserved. However, a translation by πR in the y direction remains a symmetry of the orbifold. We can see that under this transformation the even number (n = even) KK modes are invariant while the odd number (n = odd) KK modes change sign[3]. Therefore, KK parity $(-1)^n$ is still a good symmetry. This symmetry implies that the lightest KK particle (LKP) is stable and LKPs can only be pair produced. KK parity conservation plays an analogous role to R-parity conservation in supersymmetry: R-parity conservation implies that the lightest supersymmetric particle (LSP) is stable and LSPs can only be pair produced.

Electroweak symmetry breaking introduces small corrections to the KK mass spectrum, with the exception of the KK top quark excitations (top quark is much heavier). However most contributions to the splittings in the KK mass spectrum are from radiative loop corrections,

[3] KK parity is a flip of the line segment about its center at $y = \pi R/2$ combined with the Z_2 transformation which flips the sign of all odd fields.

which comprise both bulk terms and boundary terms.

The bulk terms are radiative corrections due to fields propagating along the fifth dimensions, which are finite - the corrections to the KK mass are proportional to $k/16\pi^4 R^2$ [6], where k is the contribution of the KK fields inside the loop and is different for different particles thus the KK mass degeneracy is lifted.

The boundary terms are loop effects that are localized on the fixed points of the S_1/Z_2 orbifold, which are logarithmically divergent - thus it's necessary to introduce a cutoff scale Λ, and make the assumption that all boundary terms are negligible at scale $\Lambda > R^{-1}$. The corrections to the KK mass are proportional to $m_n(k/16\pi^2)\ln(\Lambda^2/\mu^2)$ [6], where μ is the energy scale where the corrections are calculated. Thus the KK mass degeneracy is further lifted.

Assuming all boundary terms vanish at some cutoff scale $\Lambda > R^{-1}$, the MUED scenario has three free parameters:

$$\{R, \Lambda, m_h\},$$

where m_h is the mass of the SM Higgs boson, which cannot be predicted by the UED scenario.

The radiative corrections to the KK spectrum were calculated by Cheng, Matchev and Schmaltz [6] using the one-loop leading log approximation. The KK mass spectrum for the $n = 1$ KK modes is shown in Fig. 2. Fig. 3 shows the dependence of the splittings between the $n = 1$ KK modes on the cutoff scale Λ. The corrections to the masses are such that $m_{g_n} > m_{Q_n} > m_{q_n} > m_{\mathrm{W}_n} \sim m_{\mathrm{Z}_n} > m_{L_n} > m_{\ell_n} > m_{\gamma_n}$ with γ_1 being the lightest KK particle. γ_1 is a mixture of the $n = 1$ KK mode B_1 of the $U(1)_Y$ gauge boson B and the $n = 1$ KK mode W_1^0 of the $SU(2)_W$ gauge boson W^3.

The mass splitting between the KK quarks and the LKP, as well as the splitting between the weak KK gauge bosons and the LKP, were calculated by Carone, Conroy, Sher, and Turan [7] with the assumption that boundary terms vanish at the cutoff scale Λ [6]. The mass splitting as a function of $1/R$ is shown in Fig. 4, setting the value of $\Lambda R = 20$. Note that the KK W and KK Z are virtually degenerate in mass, and that $m_{\mathrm{W}}, m_{\mathrm{Z}} < m_q, m_Q$, which means the KK W and KK Z can only have leptonic decays, and result in a very clean signature for our search.

The mass splittings among the $n = 1$ KK modes are large enough for the prompt decay of a heavier $n = 1$ KK mode to a lighter $n = 1$ KK mode. But since the spectrum is still quite degenerate, the ordinary SM particles emitted from these decays will have low transverse momentum, posing a challenge for searches in a hadron collider environment.

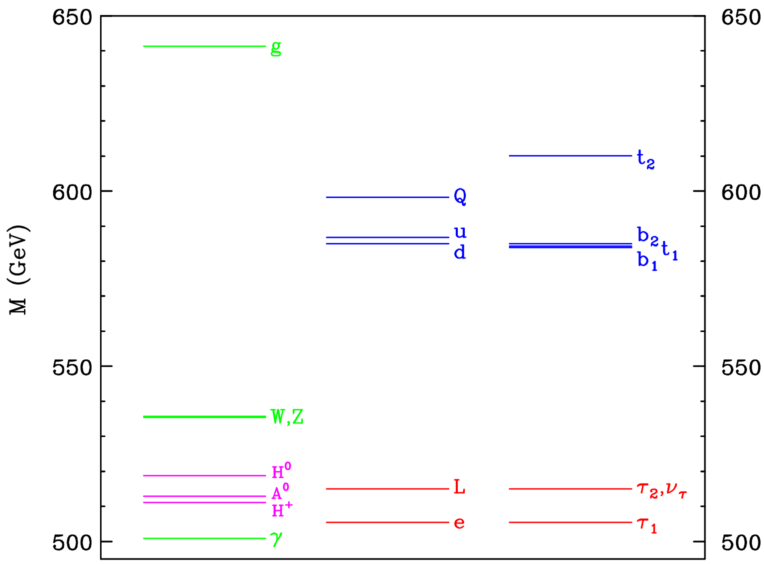

Figure 2: One-loop corrected mass spectrum of the $n = 1$ modes for $R^{-1} = 500$ GeV, $\Lambda R = 20$ and $m_h = 120$ GeV. Ref. [6]

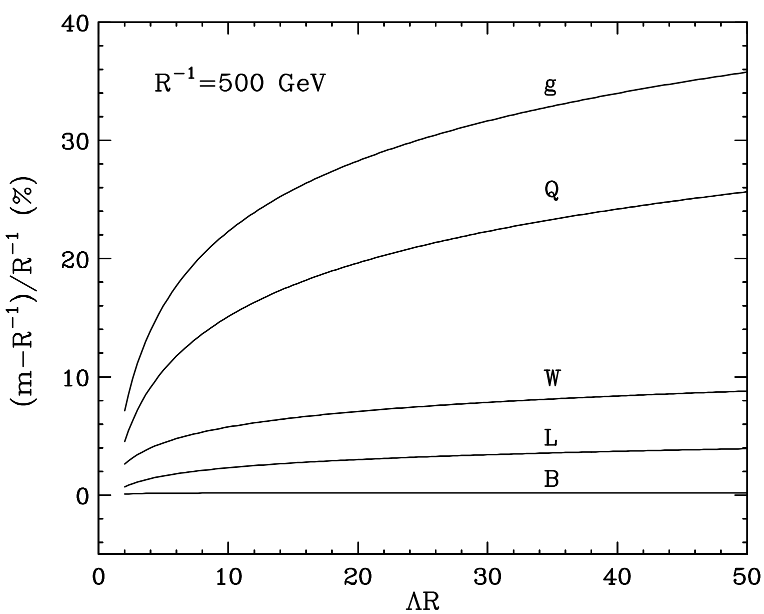

Figure 3: Radiative corrections (in %) to the spectrum of the $n = 1$ modes (gluon, quark, gauge boson W, lepton, gauge boson B) for $R^{-1} = 500$ GeV, versus ΛR. Ref. [9]

2.3 Collider Phenomenology of the MUED Scenario

The heavier $n = 1$ KK states cascade decay into the LKP by emitting soft SM particles. The cascade decay of the $n = 1$ KK modes end in the γ_1 LKP (Fig. 5 Ref [9]). The lowest level

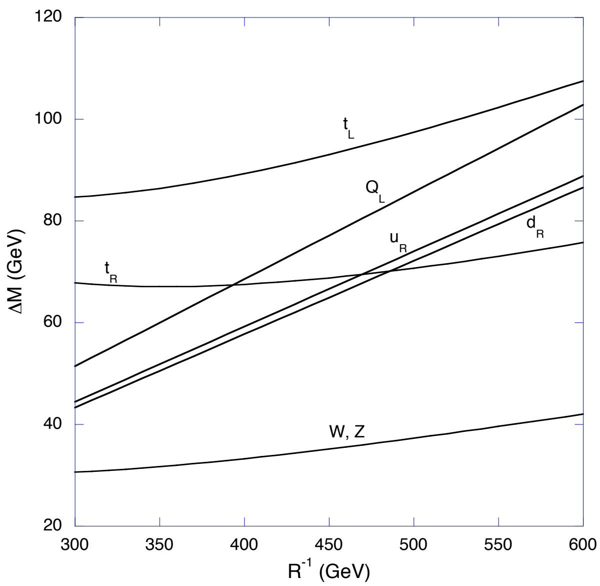

Figure 4: The mass splitting between KK quarks and the LKP $\gamma^{(1)}$, as well as the splitting between the KK gauge bosons and the LKP, as a function of $1/R$ for $\Lambda R = 20$. Here Q_L stands for all isodoublet KK quarks except top, u_R stands for up and charm isosinglet KK quarks, and d_R stands for down, strange and bottom isosinglet KK quarks. Ref. [7]

KK partners carry a conserved quantum number, KK parity, which guarantees that the LKP γ_1 is stable. The LKP γ_1 escapes detection, resulting in a missing energy signature.

At hadron colliders, KK quarks and gluons have the largest production cross section among all KK states (see Fig. 6). The $n = 1$ KK states have to be pair produced due to KK parity conservation. The cross sections at the Tevatron and the LHC are calculated in Ref. [4] and [8].

The heaviest KK particle of the $n = 1$ modes is the KK gluon g_1. It decays to a KK quark and an ordinary quark. The branching ratios are $B(g_1 \rightarrow Q_1 Q_0) \simeq B(g_1 \rightarrow q_1 q_0) \simeq 0.5$ [9].

The $SU(2)$-singlet KK quarks (q_1) will decay to the $n = 0$ mode (ordinary) quarks and a γ_1. The signature is thus jets plus missing energy ($\not{E}_T$).

The $SU(2)$-doublet KK quarks (Q_1) will mostly decay to the $n = 0$ mode (ordinary) quark and a KK W or KK Z boson. KK W or KK Z bosons will then subsequently decay to KK leptons plus ordinary leptons. KK leptons will decay to an ordinary lepton and a γ_1. The signature would be 3 leptons + 2 jets (from the $\mathrm{W}_1^{\pm}\mathrm{Z}_1$ channel), or 4 leptons + 2 jets (from the $\mathrm{Z}_1\mathrm{Z}_1$ channel) (see Fig. 7). From Ref. [9], in the limit that the Weinberg angle $\theta_W \gg \theta_1$, $sin\theta_1 \ll 1$, $B(Q_1 \rightarrow \mathrm{W}_1^{\pm} Q_0) \simeq 2B(Q_1 \rightarrow \mathrm{Z}_1 Q_0)$. Also

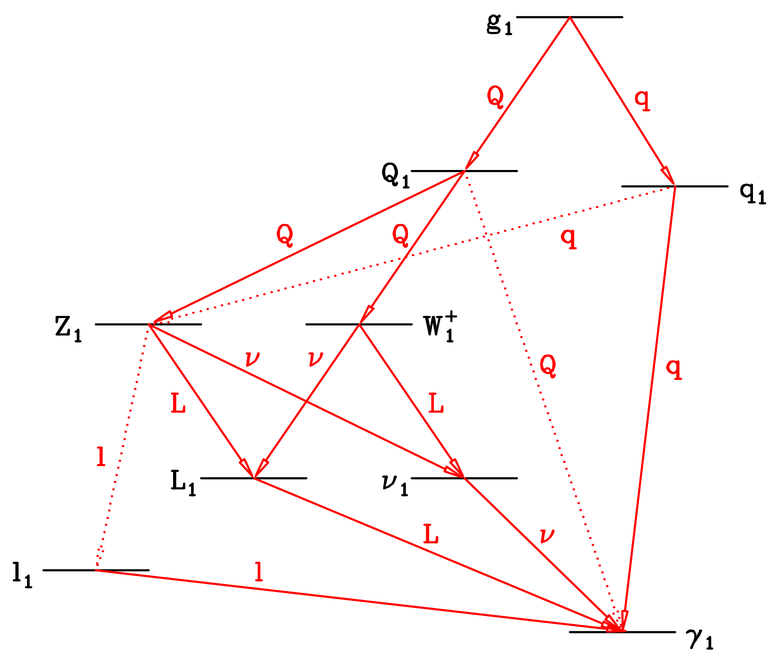

Figure 5: The $n = 1$ KK spectroscopy showing the dominant (solid) and rare (dotted) transitions and the resulting decay products. Ref [9]

$$\frac{B(Q_1 \to \mathrm{Z}_1 Q_0)}{B(Q_1 \to \gamma_1 Q_0)} \simeq \frac{g_2^2\, T_{3Q}^2\, (m_{Q_1}^2 - m_{\mathrm{Z}_1}^2)}{g_1^2\, Y_Q^2\, (m_{Q_1}^2 - m_{\gamma_1}^2)} \ , \tag{10}$$

where g_2 (g_1) is the $SU(2)_L$ ($U(1)_Y$) gauge coupling, T_3 is the weak isospin, and Y is the hypercharge. The branching ratios are: $B(Q_1 \to \mathrm{W}_1^{\pm} Q_0) \sim 65\%$, $B(Q_1 \to \mathrm{Z}_1 Q_0) \sim 33\%$ and $B(Q_1 \to \gamma_1 Q_0) \sim 2\%$ [9]. $\mathrm{W}_1^{\pm}$ and Z_1 decay to all lepton flavors with $B(\mathrm{W}_1^{\pm} \to \nu_1 L_0^{\pm}) = B(\mathrm{W}_1^{\pm} \to L_1^{\pm} \nu_0) = \frac{1}{6}$ and $B(\mathrm{Z}_1 \to L_1^{\pm} L_0^{\mp}) = B(\mathrm{Z}_1 \to \nu_1 \overline{\nu}_0) \simeq \frac{1}{6}$ for each generation. $\mathrm{Z}_1 \to l_1^{\pm} l_0^{\mp}$ decays are suppressed by $sin^2\theta_1$ so they can be neglected.

Neglecting $Q_1 \to \gamma_1 Q_0$, the branching ratios for $Q_1 \to \mathrm{W}_1$ and $Q_1 \to \mathrm{Z}_1$ are about $\frac{2}{3}$ and $\frac{1}{3}$ respectively. Table 1 lists the branching ratio in each individual channel. Clearly only channels with a check mark are contributing to the signal search in our experiment [4], and the effective ratio of $Q_1 \to \mathrm{W}_1$ to $Q_1 \to \mathrm{Z}_1$ is 4:1, thus in our signal Monte Carlo simulations we use an effective branching fraction of $B(Q_1 \to \mathrm{W}_1^{\pm} Q_0') \sim 80\%$ and $B(Q_1 \to \mathrm{Z}_1 Q_0) \sim 20\%$, and we force W_1 and Z_1 decay to the channels with a check mark only.

The final state signature for the MUED scenario at the Tevatron would be leptons, jets, plus missing energy, which is similar to the squark and gluino searches in the R-parity conserving supersymmetry models. The largest overall signature from pair produced KK

[4]Some τ's decay via channel $\tau \to \mu \overline{\nu}_\mu \nu_\tau$ and $\tau \to e \overline{\nu}_e \nu_\tau$, however the momentum of electrons/muons from these events will not be high enough to pass our lepton selection criteria.

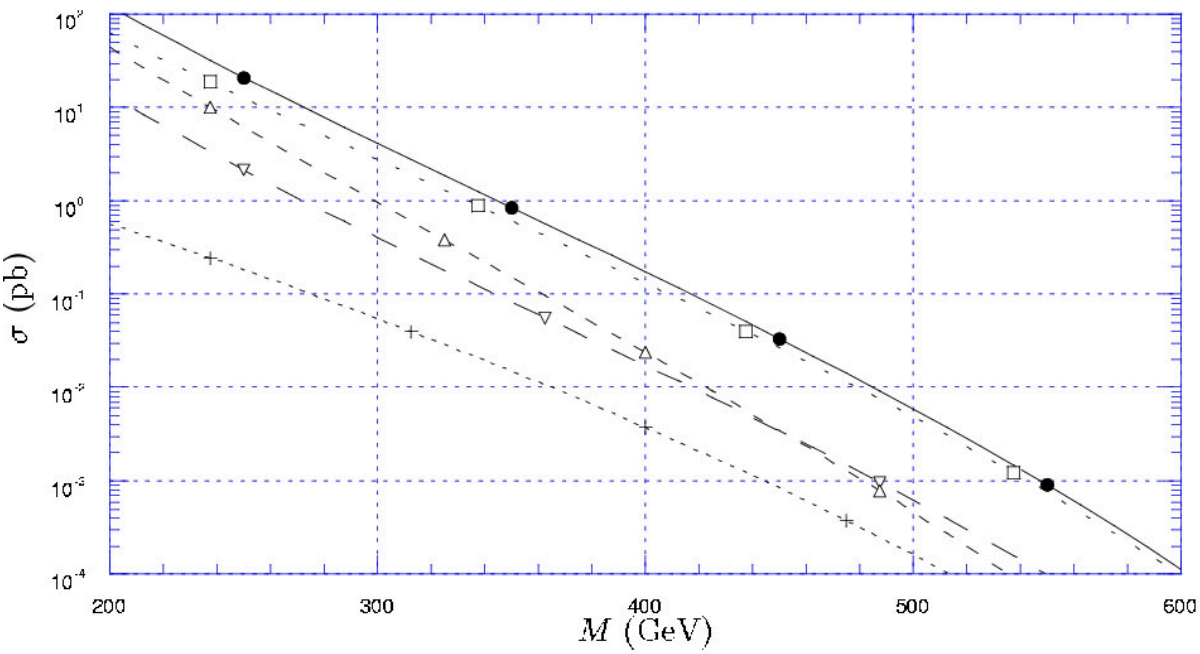

Figure 6: The cross section for the production of two stable KK final states is shown as a function of the KK mass for Tevatron Run I. The solid curve corresponds to the total contribution, while the dashed lines represent the partial contributions of KK quark pair (□), KK quark-gluon (△), and KK gluon pair (▽) production. For the case of double KK quark production, the final state consists of light quark KK excitations, excluding the top quark. Top production (+) has a different collider signature (namely, the top will subsequently decay into additional states). The production of KK quark pairs is dominant. Ref. [4]

Table 1: Q_1 decay branching ratio in each individual channel. Channels with a check mark are contributing to the signal search in our experiment.

channel	branching ratio	visible
$Q_1 \to \mathrm{W}_1 \to \nu_{1e} e_0$	$\frac{2}{3} \times \frac{1}{6}$	✓
$Q_1 \to \mathrm{W}_1 \to \nu_{1\mu} \mu_0$	$\frac{2}{3} \times \frac{1}{6}$	✓
$Q_1 \to \mathrm{W}_1 \to \nu_{1\tau} \tau_0$	$\frac{2}{3} \times \frac{1}{6}$	
$Q_1 \to \mathrm{W}_1 \to \nu_{0e} e_1$	$\frac{2}{3} \times \frac{1}{6}$	✓
$Q_1 \to \mathrm{W}_1 \to \nu_{0\mu} \mu_1$	$\frac{2}{3} \times \frac{1}{6}$	✓
$Q_1 \to \mathrm{W}_1 \to \nu_{0\tau} \tau_1$	$\frac{2}{3} \times \frac{1}{6}$	
$Q_1 \to \mathrm{Z}_1 \to e_1 e_0$	$\frac{1}{3} \times \frac{1}{6}$	✓
$Q_1 \to \mathrm{Z}_1 \to \mu_1 \mu_0$	$\frac{1}{3} \times \frac{1}{6}$	✓
$Q_1 \to \mathrm{Z}_1 \to \tau_1 \tau_0$	$\frac{1}{3} \times \frac{1}{6}$	
$Q_1 \to \mathrm{Z}_1 \to \nu_{1e} \nu_{0e}$	$\frac{1}{3} \times \frac{1}{6}$	
$Q_1 \to \mathrm{Z}_1 \to \nu_{1\mu} \nu_{0\mu}$	$\frac{1}{3} \times \frac{1}{6}$	
$Q_1 \to \mathrm{Z}_1 \to \nu_{1\tau} \nu_{0\tau}$	$\frac{1}{3} \times \frac{1}{6}$	

quarks would be at least two jets (ordinary quarks decayed from KK quarks) plus missing energy (carried away by γ_1). However the background is very large for this signal in hadron colliders. In our analysis we prefer the multilepton (ordinary electrons or muons from the $\mathrm{Z}_1\mathrm{Z}_1$ or $\mathrm{Z}_1\mathrm{W}_1$ channel) plus missing energy signature since it's much cleaner.

Pair produced $Q_1 Q_1$ (with a cross section of about $\frac{1}{4}$ total KK quark production cross section) will decay to $\mathrm{Z}_1\mathrm{Z}_1$, $\mathrm{W}_1^{\pm}\mathrm{Z}_1$ and $\mathrm{W}_1^{\pm}\mathrm{W}_1^{\pm}$. The detector signature for the $\mathrm{Z}_1\mathrm{Z}_1$ and $\mathrm{W}_1^{\pm}\mathrm{Z}_1$ events would be 4 or 3 energetic leptons respectively and substantial missing transverse energy. The main background with similar signature comes from $b\bar{b}/c\bar{c}$, $t\bar{t}$, WZ, ZZ production, and Drell-Yan and WW production with misidentified leptons. In order to study techniques for rejecting background, we use Monte Carlo techniques to study a large number of events of both signal and background processes. Details are discussed in Chapter 5.

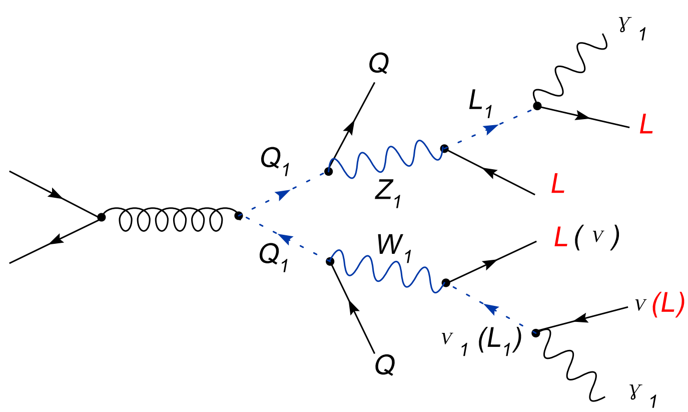

Figure 7: UED in 3 or 4 lepton modes. The signature would be 3 leptons + 2 jets ($W_1^{\pm}Z_1$), or 4 leptons + 2 jets (Z_1Z_1).

3 Data Samples

The data used for this analysis were taken with the Collider Detector at Fermilab (CDF) in the years 1994-1996 (Run 1B). For a description of the CDF detector, see Ref. [10]. We start with the same data set as the CDF trilepton analysis [11], and impose the same trilepton skimming cuts to reduce the size of the data sample. We obtained the same sample size during the process: Run IB SUSY dilepton data set has 457,478 events, reduced from the 3,270,488-event XDLB_5P data set, and 15,149 events pass the trilepton skimming cuts. Next we imposed similar analysis cuts except that we did not require leptons to be isolated [5] because leptons of MUED signal are not well isolated (as determined from our Monte Carlo study, see Fig. 22). We obtained 1120 events after our trilepton analysis cuts, which is a larger sample compared with 247 events of the CDF trilepton analysis [19].

3.1 Run IB Dilepton Sample

We begin with the 87.5 pb^{-1} Run IB exotic dilepton data set XDLB_5P. This data set is created using the TDLFLT module[6], which requires events to have a central electron ($|\eta^e| < 1.1$) with $E_T > 8$ GeV or central muon ($|\eta^\mu| < 0.6$) with $\mathrm{p_T} > 8$ GeV/c and a second electron ($|\eta^e| < 2.4$) with $E_T > 3$ GeV or muon ($|\eta^\mu| < 1.0$) with $\mathrm{p_T} > 3$ GeV/c. This data set contains 3,270,488 events and is written on 63 tapes.

Next, the Run IB SUSY dilepton data set [13] is selected from the exotic dilepton sample by requiring:

- At least one central lepton (CEM, CMU, CMP)[7] passing tight requirements listed in Table 2 (electron) or Table 3 (muon).
- At least one additional lepton (CEM, PEM, CMU, CMP, CMX, CMIO)[8] passing loose requirements listed in Table 2 (electron) or Table 3 (muon).

Note that no isolation cut is applied. The requirements are explained in Appendix B.

A total of 457,478 events [9] are selected for the Run IB SUSY dilepton data set. This is the starting sample for our analysis.

[5] Isolation in this analysis is defined as the energy in a cone of $\Delta R \equiv \sqrt{\Delta\phi^2 + \Delta\eta^2} = 0.4$ minus the electron or muon energy.

[6] TDLFLT module utilizes the level 3 exotic dilepton trigger (COMBINED_EXOB_DIL [12]).

[7] CEM stands for Central ElectroMagnetic calorimeter. CMU stands for Central MUon detector. CMP stands for Central Muon uPgrade detector.

[8] PEM stands for Plug ElectroMagnetic calorimeter. CMX stands for Central Muon eXtension detector. CMIO stands for Central Minimum Ionizing Object.

[9] These events are written on 8 tapes: RK8876, RK8880, RK8885, RK8895, RK8897, RK8899, RK8921, RK9198.

Table 2: Selection criteria for electrons (CEM, PEM). Electron candidates are categorized as Tight Central Electron (TCE), Loose Central Electron (LCE) and Loose Plug Electron (LPE).

Lepton	Tight	Loose	
Cut variables	TCE	LCE	LPE
p_T (GeV/c)	≥ 6.0	≥ 2.8	—
E_T (GeV)	≥ 8.0	≥ 4.0	≥ 4.0
E/p	≤ 2.0	≤ 2.0	—
E_{HAD}/E_{EM}	≤ 0.05	$\leq 0.055 + 0.045 \times \frac{E}{100}$	≤ 0.1
L_{SHR}	≤ 0.2	≤ 0.2	—
$\lvert\Delta x\rvert$ (cm)	≤ 3.0	≤ 3.0	—
$\lvert\Delta z\rvert$ (cm)	≤ 5.0	≤ 5.0	—
χ^2_{strip}	≤ 10.0	≤ 15.0	—
$\chi^2_{3\times 3}$	—	—	≤ 3.0
VTX Occupancy	—	—	≥ 0.5

Table 3: Selection criteria for muons (CMU, CMP, CMX, CMIO). Muon candidates are categorized as Tight Central Muon (TCM), Loose Central Muon (LCM), Loose eXtension Muon (LXM) and Loose CMIO Muon (LMI).

Lepton	Tight	Loose		
Cut variables	TCM	LCM	LXM	LMI
p_T (GeV/c)	≥ 7.5	≥ 2.8	≥ 2.8	≥ 10
E_{EM} (GeV)	≤ 2.0	≤ 2.0	≤ 2.0	≤ 2.0
E_{HAD} (GeV)	≤ 6.0	≤ 6.0	≤ 6.0	≤ 6.0
d_0 raw (cm)	≤ 0.5	≤ 0.8	≤ 0.8	≤ 0.8
CMU Matching	$\lvert\Delta x\rvert \leq 2$ cm or $\chi^2_{CTC} \leq 9$	$\lvert\Delta x\rvert \leq 2$ cm or $\chi^2_{CTC} \leq 9$	—	—
CMP Matching	$\lvert\Delta x\rvert \leq 5$ cm or $\chi^2_{CTC} \leq 9$	$\lvert\Delta x\rvert \leq 5$ cm or $\chi^2_{CTC} \leq 9$	—	—
CMX Matching	—	—	$\lvert\Delta x\rvert \leq 5$ cm or $\chi^2_{CTC} \leq 9$	—

3.2 Run IB Trilepton Skimming Selection

Next we require that events have a third lepton passing loose requirements listed in Table 2 (electron) or Table 3 (muon). Thus our trilepton skimming selection requires:

- At least one central lepton (CEM, CMU, CMP) passing tight requirements listed in Table 2 (electron) or Table 3 (muon).
- Two additional leptons (CEM, PEM, CMU, CMP, CMX, CMIO) passing loose requirements listed in Table 2 (electron) or Table 3 (muon).

A total of 15,149 events passed our trilepton skimming cuts.

3.3 Run IB Trilepton Analysis Selection

Our skimmed trilepton data sample still contains a significant fraction of events that are not candidates for our search. We further clean up our sample by imposing tighter identification cuts listed in Tables 4 and 5 for electrons and muons.

Electron identification cuts

E_T is increased from 8 GeV to 11 GeV for the tight electron and from 4 GeV to 5 GeV for the loose electron. This change will reject more background events with minimal effect on signal acceptance.

Conversion removal is to remove electrons that are from photon conversion. An electron is rejected if there are two opposite-sign tracks pointing to the electron cluster, since it is likely a photon that converted in the solenoid material.

Fiducial Area requires the electron is in a region that CEM or PEM is known to function well.

Muon identification cuts

$\mathrm{p_T}$ is increased from 7.5 GeV to 11 GeV/c for tight CMU/P muon and from 2.8 GeV/c to 4 GeV/c for loose CMU/P or CMX muon. This change will reject more background events with minimal effect on signal acceptance.

Table 4: Analysis lepton selection cuts for CEM and PEM electrons.

Lepton	Tight	Loose	
Cut variables	TCE	LCE	LPE
E_T (GeV)	≥ 11	≥ 5	≥ 5
E/p	≤ 2	≤ 2	—
HAD/EM	≤ 0.05	$\leq 0.055 + 0.045 \times \frac{E}{100}$	≤ 0.1
L_{SHR}	≤ 0.2	≤ 0.2	—
$\|\Delta x\|$ (cm)	≤ 3	≤ 3	—
$\|\Delta z\|$ (cm)	≤ 5	≤ 5	—
χ^2_{strip}	≤ 10	≤ 15	—
$\chi^2_{3\times3}$	—	—	≤ 3
VTX occupancy	—	—	≥ 0.5
Conversion removal	Yes	Yes	Yes
Fiducial Area	Yes	Yes	Yes

Table 5: Analysis lepton selection cuts for CMU/P, CMX and CMIO muons.

Lepton	Tight	Loose		
Cut variables	TCM	LCM	LMX	LMI
p_T (GeV/c)	≥ 11	≥ 4	≥ 4	≥ 10
EM (GeV)	≤ 2	≤ 2	≤ 2	≤ 2
Had (GeV)	≤ 6	≤ 6	≤ 6	≤ 6
d_0 raw (cm)	≤ 0.5	≤ 0.8	≤ 0.8	≤ 0.8
d_0 beam (cm)	≤ 0.2	≤ 0.5	≤ 0.5	≤ 0.5
CMU Matching	$\|\Delta x\| \leq 2$ cm or $\chi^2_{CTC} \leq 9$	$\|\Delta x\| \leq 2$ cm or $\chi^2_{CTC} \leq 9$	—	—
CMP Matching	$\|\Delta x\| \leq 5$ cm or $\chi^2_{CTC} \leq 9$	$\|\Delta x\| \leq 5$ cm or $\chi^2_{CTC} \leq 9$	—	—
CMX Matching	—	—	$\|\Delta x\| \leq 5$ cm or $\chi^2_{CTC} \leq 9$	—
EM+Had (GeV)	≥ 0.1	≥ 0.1	≥ 0.1	≥ 0.1
Not Fiducial Area	—	—	—	Yes

d_0 **raw** is the impact parameter *i.e.* the distance of the closest approach of the reconstructed track to the beam line. In early CDF trilepton analysis [19] this cut is tightened from 0.8 cm to 0.5 cm for loose CMU/P, CMX or CMIO muons, however it is not necessary to tighten this cut because d_0 beam cut will be used. Later multi-lepton analysis don't tighten d_0 raw cut, and we don't tighten this cut in this analysis either.

d_0 **beam** is the beam constrained impact parameter which is determined by using the beam position (in z). We require a tight CMU/P muon to have d_0 beam $\leqslant 0.2$ cm and a loose CMU/P, CMX or CMIO muon to have d_0 beam $\leqslant 0.5$ cm.

EM + Had requires the muon deposit at least 100 MeV in the calorimeters.

Not Fiducial Area requires that a CMIO muon does not point at a muon chamber, since it would have made a muon stub otherwise.

All of these requirements are the same as used in the CDF trilepton analysis [19] except those we have mentioned above (isolation requirement and d_0 raw). After the 3 lepton analysis requirements we are left with 1120 events.

4 Standard Model Backgrounds

There are several SM processes which can produce a multi-lepton final state. The main source of multi-lepton events are events with three or more real leptons, and events with two real leptons plus a misidentified lepton. This misidentified lepton may come from unrelated parts of the event, e.g. a real lepton from the underlying event, or a hadronic track misidentified as a lepton. Events with three real leptons include $W^{\pm}Z^0$, Z^0Z^0, $t\bar{t}$ and $b\bar{b}$. Events with two real leptons include $W^{\pm}W^{\mp}$, $c\bar{c}$ and Drell-Yan (γ^* and Z^0). Some of these background sources have very small production cross sections while other background have distinctive signatures. In addition, cosmic rays constantly passing through our detector manifest themselves as dimuon events with back-to-back CTC tracks, thus become a substantial background to our analysis [10]. By comparing the kinematics of signal and background events, we can use a series of cuts to reject background with minimal effect on signal acceptance.

In order to determine the contribution of real leptons from the SM processes to the signal we used the CDF SUSY group MC samples (Appendix D). Branching ratio numbers in this section are from Particle Data Group, and production cross section numbers are from various CDF publications.

4.1 Real multi-lepton events

Processes that can produce three or more real leptons include

1. $b\bar{b}$ Production
2. $t\bar{t}$ Production
3. Dibosons (ZZ, WZ) Production

In our analysis we count real multi-lepton background events by requiring at least one central lepton passing tight requirements listed in Table 4 or Table 5 and two additional leptons passing loose requirements listed in Table 4 or Table 5. [11]

$b\bar{b}$ Production A typical b decay is $b \to Wc \to W(Wd)$. Each W has 11% chance of decaying to an e and 11% chance of decaying to a μ. Thus the probability of both Ws decay leptonically is about 4%. If either of the W from the $\bar{b}$ also decays leptonically, we will have three real leptons in the event. Since b quarks are copiously produced at the Tevatron (the

[10] CDF Run IB detector simulation program QFL can not properly simulate cosmic muons.

[11] It is possible that events with a hadron passing the requirements are included and those events will be removed with later cuts.

production cross section for $b\bar{b}$ is very high: $\sigma = 3.52 \pm 0.38(stat) \pm 0.46(syst) \times 10^6$ pb [14]), $b\bar{b}$ can be a substantial background. We are able to remove most $b\bar{b}$ (and $c\bar{c}$) background by requiring the invariant mass of the two closest[12] leptons to be greater than 5 GeV/c^2 (see Fig.8).

Since the MUED signal event has at least one opposite sign pair of the same flavor leptons, while the flavor of the leptons from the b and c decays are not correlated, we require at least one opposite sign pair of the same flavor leptons to further reduce $b\bar{b}$, $c\bar{c}$ background in the invariant mass > 5 GeV/c^2 region.

$t\bar{t}$ Production A top quark will decay $t \to W^{\pm}b$ in the SM. We can get at most two leptons from the $W^{\pm}$ decays (one from the t and one from the $\bar{t}$) and at least one of the three leptons is from the semi-leptonic decay of a b. The production cross section for $t\bar{t}$ is $6.5^{+1.7}_{-1.4}$ pb [15], so small that this background is negligible.

Diboson Production: Z^0Z^0 and $W^{\pm}Z^0$ Both the production cross section for Z^0Z^0 ($\sigma(ZZ) = 1.08$ pb [16], BR = 0.45% to e or μ) and $W^{\pm}Z^0$ ($\sigma(WZ) = 2.5$ pb [16], BR = 1.44% to e or μ) and the branching ratio to three lepton final states are small. However, the leptons from either Z^0Z^0 or $W^{\pm}Z^0$ are kinematically very similar to those from our signal events, so we must be able to remove this type of background. Both of these types of events contain a Z^0, so we can use a Z^0 mass window cut to remove them. We remove an event if any same-flavor opposite-sign lepton-pair two-body masses are in the range 76 GeV/c^2 $\leqslant M_{\ell\ell} \leqslant$ 106 GeV/c^2.

4.2 Dilepton plus misidentified lepton events

Processes which can produce two real leptons include Drell-Yan (γ^* and Z^0) and W^+W^- production.

Drell-Yan (Z^0 and γ^*) Production The Drell-Yan background can be split up into three categories: γ^* production ($\overline{q}q \to \gamma^* \to l^+l^-$), and low- and high-p$_{\mathrm{T}}$ Z^0 production ($\overline{q}q \to Z^0 \to l^+l^-$). The high mass Drell-Yan events (with Z^0 mediator) production cross section from the CDF published measurement is: $\sigma(Z^0) = 6.94 \pm 0.53$ nb and $\sigma \cdot Br(Z^0 \to \mu^+\mu^-) = 233 \pm 18$ pb [17]. The low mass Drell-Yan events (with γ^* mediator) production cross section from the CDF published measurement is 259 ± 57 pb [18]. Events from γ^* production can be removed with an opening angle cut. Low-p$_{\mathrm{T}}$ Z^0 will produce leptons that are back-to-back, so they can also be removed with an opening angle cut. Leptons from high-p$_{\mathrm{T}}$ Z^0 decays will not be back to back so we remove them with a Z^0 mass window cut.

[12] We calculated the spatial angles between any two of the three lepton candidates regardless of charge or flavor, and choose the two leptons that form the smallest angle to calculate the invariant mass.

To remove this type background, we require the opening angle between the two highest $\mathrm{p_T}$ leptons be less than 2.96 radians (170°). In addition we require the event not have a same-flavor opposite-sign lepton-pair two-body mass in the range 76 GeV/c$^2 \leqslant M_{\ell\ell} \leqslant$ 106 GeV/c^2.

W^+W^- **Production** W^+W^- production has a low production cross section ($\sigma(WW)$ = 9.53 pb [16]). For an event from W^+W^- production to be accepted, it must also have a fake lepton. Thus, the probability of such an event contaminating our sample is small. Each $W^\pm$ can decay to either e or μ with equal probability. We can reduce this background by 50% by requiring such a pair of leptons.

Measurement of the misidentified lepton rate There are several methods to calculate the fake lepton rate. The calculation can be based on the overall number of events or on an event-by-event basis. For the first approach, we use a sample with the assumption that the hard processes and the structure of the events in the sample and the data are similar, to get a prediction for the fake rate.

For the CDF-trilepton analysis [19], such a study based on the $W^\pm$ sample [20] was performed. Two analysis modules CleanW and LeptCount were used. CleanW filter prepares a sample of W events; LeptCount counts the leptons, apart from the W leptons, which pass the same lepton ID cuts described above with further requirements:

- a lepton with $\mathrm{p_T} > 20$ GeV/c,
- missing transverse energy $\not\!\!E_T > 20$ GeV,
- a transverse mass of lepton: 40 GeV/c$^2 < M_T(\mathrm{p_T}, \not\!\!E_T) <$ 100 GeV/c^2.

Any event passing these cuts we call a $W^\pm$.

In 21 pb^{-1} of Run IB data, 16,596 events passed CleanW filter: 10,861 $W^\pm \to e\nu$ and 5,735 $W^\pm \to \mu\nu$, and 48 fake leptons were found by LeptCount, never more than one per event. Thus the probability that a $W^\pm$ event will contain a fake lepton is 0.289±0.042%. Since no events with two fake leptons were found, background from (single lepton + two fakes) is not considered.

The fake lepton rate has been re-examined in the CDF multi-lepton analysis [28]. In this study leptons are not required to be isolated, and as a result a higher number of leptons are found: 68 events containing CEM electrons and 73 events containing CMUO muons out of 17,336 events passing CleanW filter. Thus the fake lepton rate is 0.81±0.07%.

Assuming no $\mathrm{p_T}$ dependence on the rate of fake leptons, we use 0.81±0.07% as the probability that any event will have a fake lepton.

To calculate the number of multi-lepton events due to (dilepton + fake) we require one tight lepton and one loose lepton. We then use the probability of each event having a fake lepton times the number of dilepton events as the number of expected background due to (dilepton + fake).

5 Monte Carlo Simulations

We use the Monte Carlo (MC) techniques to obtain a large number of events of both MUED signal and background processes. Event generators (ISAJET [21], PYTHIA [22], etc.) simulate the desired process and write the events to a generator level data bank [13] which contains momentum, energy, flavor, charge, parent, daughter etc. information for every particle generated in the event. CDF Run I uses YBOS format and Run II uses ROOT format. The conversion between YBOS format and ROOT format can be done using standard CDF Run II module BankTools [14]. Detector effects (such as resolution and smearing) are addressed by detector simulation. All simulated events used in this analysis were processed with a fast CDF detector simulation software QFL [23]. After generation and QFL detector simulation, the events have the same format as data taken with the detector. Thus we can use the same program to analyze both data and Monte Carlo events.

5.1 MUED Signal Simulation

We have studied the MUED scenario by using Pythia 6.203 to produce MC samples with various radii of the extra dimension R^{-1} (see Appendix E for an example Pythia tcl file). We used the default Pythia structure function CTEQ-5L. In order to reduce the statistical uncertainties, at each MC point we generated about 25,000 signal events (more than 20 times larger than we would expect in our actual data).

We examined mass spectra of $n = 1$ KK particles for different choices of R^{-1} and Λ as listed in Table 6. The relevant formulas used to calculate the radiative corrections to KK masses are listed in Appendix A.

We are interested in 3-lepton (from $W_1^{\pm}Z_1$) or 4-lepton (from Z_1Z_1) events. With effective branching fraction of $B(Q_1 \rightarrow W_1^{\pm}Q_0') \sim 80\%$ and $B(Q_1 \rightarrow Z_1Q_0) \sim 20\%$, a KK quark pair will have a 4% chance decay to Z_1Z_1 pair, a 32% chance decay to $W_1^{\pm}Z_1$ pair, and a 64% chance decay to $W_1^{\pm}W_1^{\mp}$ pair.

5.2 The Standard Model Background Simulation

The SUSY working group has generated large background Monte Carlo samples for Run 1b analyses with ISAJET version 7_06 and 7_20. Five different structure functions have been used in the generation. Each MC sample corresponds to a different integrated luminosity and the number of MC events need to be scaled before comparing with the data. The contribution of background in each category ($b\bar{b}/c\bar{c}$, Drell-Yan, boson pair, $t\bar{t}$) is obtained by averaging

[13] GENP bank for ISAJET and HEPG bank for PYTHIA.
[14] http://cdfkits.fnal.gov/CdfCode/source/BankTools/

Table 6: Monte Carlo points examined for $n = 1$ KK particles of different values of R^{-1} (GeV) and ΛR. Higgs mass is fixed at $m_h = 120$ GeV. The relevant formulas used to calculate the radiative corrections to KK masses are listed in Appendix A.

R^{-1}	ΛR	M_{γ_1}	M_{L_1}	M_{W_1}	M_{Z_1}	M_{Q_1}	M_{g_1}
250	20	250.3	257.0	276.6	276.9	298.4	320.5
250	50	250.4	259.1	280.7	281.0	313.2	339.1
300	20	300.3	308.3	327.6	327.8	358.1	384.6
300	50	300.3	310.9	332.6	332.8	375.8	406.9
350	20	350.3	359.7	379.1	379.2	417.7	448.7
350	50	350.3	362.7	385.1	385.2	438.5	474.8
400	20	400.2	411.1	431.0	431.1	477.4	512.7
400	50	400.2	414.5	437.8	437.9	501.1	542.6
450	20	450.2	462.5	483.1	483.2	537.1	576.8
450	50	450.2	466.3	490.8	490.9	563.7	610.4
500	20	500.2	513.9	535.4	535.4	596.8	640.9
500	50	500.2	518.2	543.9	544.0	626.4	678.2

over structure functions and then summing over runs. The total expected background is the sum of all categories. For details on SUSY working group Run 1B SM background simulation see Appendix D.

5.3 Monte Carlo Efficiency Corrections

Our detector simulation program QFL does not model trigger efficiencies or isolation efficiencies, and tends to be over-efficient in lepton identification. Thus we need to determine those corrections and apply them to both signal and background MC events.

5.3.1 Trigger Efficiencies

The data needs to pass various triggers to enter the final data set. In order to compare MC events with data, we need to check each lepton candidate of the MC event to determine which triggers it would have most likely activated.

A trigger efficiency study has been done in Ref. [19]. Each individual trigger's efficiency is coded into trigger simulation routine MC_WGT. The trigger efficiency correction of the MC events are determined on an event-by-event basis: for each event, the lepton candidate's $E_T(P_T)$ and η are examined, and the routine MC_WGT returns the Level 1 trigger efficiency, the Level 2 trigger efficiency and the Level 3 trigger efficiency. The total trigger efficiency of this MC event is the product of three different trigger level efficiencies, and it is the weighting factor that needs to be applied to this event. The trigger efficiency correction is applied to both the background and signal MC calculation.

5.3.2 Lepton Identification Efficiencies

QFL tends to overestimate the lepton identification efficiency due to not including subtle detector efforts (such as detector aging). The efficiency corrections including lepton identification, conversion electron removal, "good" CTC track requirement, and cosmic muon removal have been studied in Ref. [24].

In Table 7 we summarize the detector-by-detector detection efficiencies for data and MC, and correction factors. We want to obtain an overall lepton identification efficiency correction factor that will be applied to every MC event, rather than an event-by-event correction since the differences are small. We take the most conservative approach and combine the correction factors that will give us the largest correction (that deviates from 1). For our analysis, an event with a central electron that passes the tight lepton ID cuts, and two loose electrons that pass the loose electron ID cuts will likely have the largest correction. The overall correction factor is 0.86 ± 0.02 ($\pm2\%$) ($0.944 \times 0.954 \times 0.954 = 0.86$, $\sqrt{(1.08\%)^2 + (1.00\% + 1.00\%)^2} = 2\%$, $0.86 \times 2\% = 0.02$). This factor is applied to both the background and signal MC calculation.

Table 7: Summary of efficiencies including lepton identification, photon-conversion removal (TCE and LCE only), "good" CTC track (not LPE), and cosmic ray removal (muons only). data/MC is used to calculate the efficiency correction factor for the Monte Carlo. Leptons are categorized by Tight Central Electron (TCE), Loose Central Electron (LCE), Loose Plug Electron (LPE), Tight Central Muon (TCM), Loose Central Muon (LCM), Loose eXtension Muon (LXM) and Loose CMIO Muon (LMI). Table 16 of Ref. [24] lists Eff. (Drell-Yan MC) and Eff. (Run IB Z^0 inclusive electron and muon data sample) with absolute uncertainties, we have calculated IB/MC and all relative uncertainties in this table.

	Eff. (Drell-Yan MC)	Eff. (Run IB Z^0 data sample)	Correction (data/MC)
TCE	0.863 ± 0.004 (0.46%)	0.815 ± 0.008 (0.98%)	0.944 ± 0.010 (1.08%)
LCE	0.888 ± 0.003 (0.34%)	0.847 ± 0.008 (0.94%)	0.954 ± 0.010 (1.00%)
LPE	0.924 ± 0.004 (0.43%)	0.920 ± 0.007 (0.76%)	0.996 ± 0.009 (0.87%)
TCM	0.977 ± 0.003 (0.31%)	0.929 ± 0.007 (0.75%)	0.951 ± 0.008 (0.81%)
LCM	0.976 ± 0.003 (0.31%)	0.937 ± 0.006 (0.64%)	0.960 ± 0.007 (0.71%)
LMX	0.957 ± 0.005 (0.52%)	0.929 ± 0.010 (1.08%)	0.971 ± 0.012 (1.19%)
LMI	0.880 ± 0.008 (0.91%)	0.912 ± 0.014 (1.54%)	1.036 ± 0.019 (1.79%)

5.3.3 Isolation Efficiencies

QFL does not simulate lepton isolation correctly due to multiple interactions at high instantaneous luminosity. Efficiencies of calorimeter and track isolation cuts for leptons are determined using the Run 1B Z^0 events in Ref. [25]. For calorimeter isolation cuts at 4 GeV with the presence of 2 jets, the isolation correction factors for electrons and muons can be obtained from comparing the last columns of Table 8 and Table 9. We are cutting on the maximum isolation of the three lepton candidates for our analysis, thus an event with a muon having the maximum isolation will result in the largest isolation efficiency correction of 0.92 (0.904/0.980), with relative uncertainty of 4.7% ($\sqrt{(0.041/0.904)^2 + (0.011/0.980)^2} = 4.7\%$). We only apply isolation requirement at the final stage of our analysis.

Table 8: Summary of calorimeter isolation efficiency $ISO^{cal} < 4$ GeV for jet multiplicity of cone size R = 0.7 (0.4) of Run IB Z^0 data events. From Table 9 of Ref. [25].

Object	$\eta_j^{0.7(0.4)} = 0$	$\eta_j^{0.7(0.4)} = 1$	$\eta_j^{0.7(0.4)} \geqslant 2$
e^{CEM}	0.970 ± 0.005 (0.970 ± 0.004)	0.958 ± 0.010 (0.956 ± 0.012)	0.953 ± 0.021 (0.936 ± 0.028)
e^{PEM}	0.981 ± 0.003 (0.977 ± 0.004)	0.962 ± 0.009 (0.967 ± 0.010)	0.941 ± 0.022 (0.971 ± 0.020)
μ	0.970 ± 0.005 (0.971 ± 0.005)	0.967 ± 0.010 (0.966 ± 0.011)	0.937 ± 0.027 (0.904 ± 0.041)

Table 9: Summary of calorimeter isolation efficiency $ISO^{cal} < 4$ GeV for jet multiplicity of cone size R = 0.7 (0.4) of ISAJET+QFL Drell-Yan MC events. From Table 13 of Ref. [25].

Object	$\eta_j^{0.7(0.4)} = 0$	$\eta_j^{0.7(0.4)} = 1$	$\eta_j^{0.7(0.4)} \geqslant 2$
e^{CEM}	0.981 ± 0.002 (0.991 ± 0.002)	0.987 ± 0.004 (0.990 ± 0.004)	0.967 ± 0.012 (0.994 ± 0.006)
e^{PEM}	0.995 ± 0.001 (0.995 ± 0.001)	0.993 ± 0.002 (0.995 ± 0.003)	0.985 ± 0.009 (0.991 ± 0.009)
μ	0.986 ± 0.002 (0.989 ± 0.002)	0.991 ± 0.003 (0.985 ± 0.004)	0.991 ± 0.008 (0.980 ± 0.011)

6 Data Analysis

Our analysis includes the identification of events with three good leptons and the rejection of standard model background events.

6.1 Bad Run Removal

In addition to the lepton identification cuts there are several new constraints. Our data sample includes events from runs in which part of the detector was turned off or the data were taken with bad beam conditions. All events from these runs were rejected using the CDF standard offline routine BADRUN[26]. This routine checks a database containing information about the state of the detector during a data taking run. We only accept runs for which BADRUN reports a fully operational detector.

After removing bad runs we are left with 1068 events.

6.2 Cosmic Ray Removal

Cosmic rays are constantly passing the atmosphere and they create showers of particles which often decay to muons. These muons passing through our detector are a substantial background to our analysis.

From the detector's point of view, a cosmic ray manifests itself as a dimuon event with CTC tracks that are back-to-back in η and ϕ, and often has a large impact parameter. In addition, since the cosmic ray travels through the detector (rather than originating at the interaction point and travelling outward), the difference in the timing signals measured by the Time to Digital Converter (TDC) for the two legs will be roughly equal to the speed-of-light transit time from one side of the calorimeter to the other.

Two techniques are used to remove cosmic rays: a CDF standard routine CMCOS [27] and a custom routine that examines the opening angle between the muons[15] and the difference in the time when each particle passed through the hadron calorimeter[16].

CDF Run IB detector simulation program QFL does not properly simulate the hadron calorimeter TDC (HTDC). Therefore cosmic ray removal is not applied to MC samples.

After cosmic removal, we are left with 750 events.

[15]Events are removed if the opening angle is greater than 3 radians

[16]Events are removed if the difference in time for the two opposite muons is greater than 12 ns

6.3 Vertex Requirements

The primary vertex for an event is the $p\bar{p}$ interaction point. We impose two vertex requirements:

- All three leptons have $z_{vertex} < 60$ cm, to ensure high quality tracks in the CTC.
- All three leptons are associated with tracks that are within 10 cm of the same z-vertex, to remove events with leptons that do not originate from the primary vertex. This is not applied to PEM electrons because they may not be associated with a good track.

After vertex requirements we are left with 683 events.

6.4 Charge Sum and Lepton Pair Requirements

Events of interest are 3-lepton ($W_1^{\pm}Z_1$ channel) or 4-lepton (Z_1Z_1 channel) events, thus we expect at least one e^+e^- or $\mu^+\mu^-$ pair from the three lepton candidates with their charges satisfy $|q_1 + q_2 + q_3| < 3$.

After charge sum and lepton pair requirements we are left with 545 events.

6.5 Invariant Mass Requirements

$b\bar{b}/c\bar{c}$ background events are a substantial background to our analysis (see section 4.1). We require the invariant mass of the two closest [17] leptons to be greater than 5 GeV/c^2 (see Fig. 8). This allows us to reject $b\bar{b}/c\bar{c}$ background without sacrificing much of the signal. Our result shows that this cut also removes all e^+e^- or $\mu^+\mu^-$ events that originate from the J/ψ.

After invariant mass requirements we are left with 68 events.

By looking at Fig. 8, we noticed that in the invariant mass less than 5 GeV/c^2 region where $b\bar{b}/c\bar{c}$ background dominates, the background Monte Carlo and data do not agree with each other. The $b\bar{b}/c\bar{c}$ background was not modeled correctly because old structure functions were used, thus an overall scale factor needs to be applied to $b\bar{b}/c\bar{c}$ background. This scale factor is determined to be 2.1 (see Appendix F), which is then applied to the $b\bar{b}/c\bar{c}$ background over the entire mass range. For the remainder of this analysis the scale factor 2.1 is applied to $b\bar{b}/c\bar{c}$ background, and the total background includes $b\bar{b}/c\bar{c}$ background with scale factor 2.1 applied, Drell-Yan, $t\bar{t}$, and boson pairs.

[17] We calculated the spatial angles between any two of the three lepton candidates regardless of charge or flavor, and choose the two leptons that form the smallest angle to calculate the invariant mass.

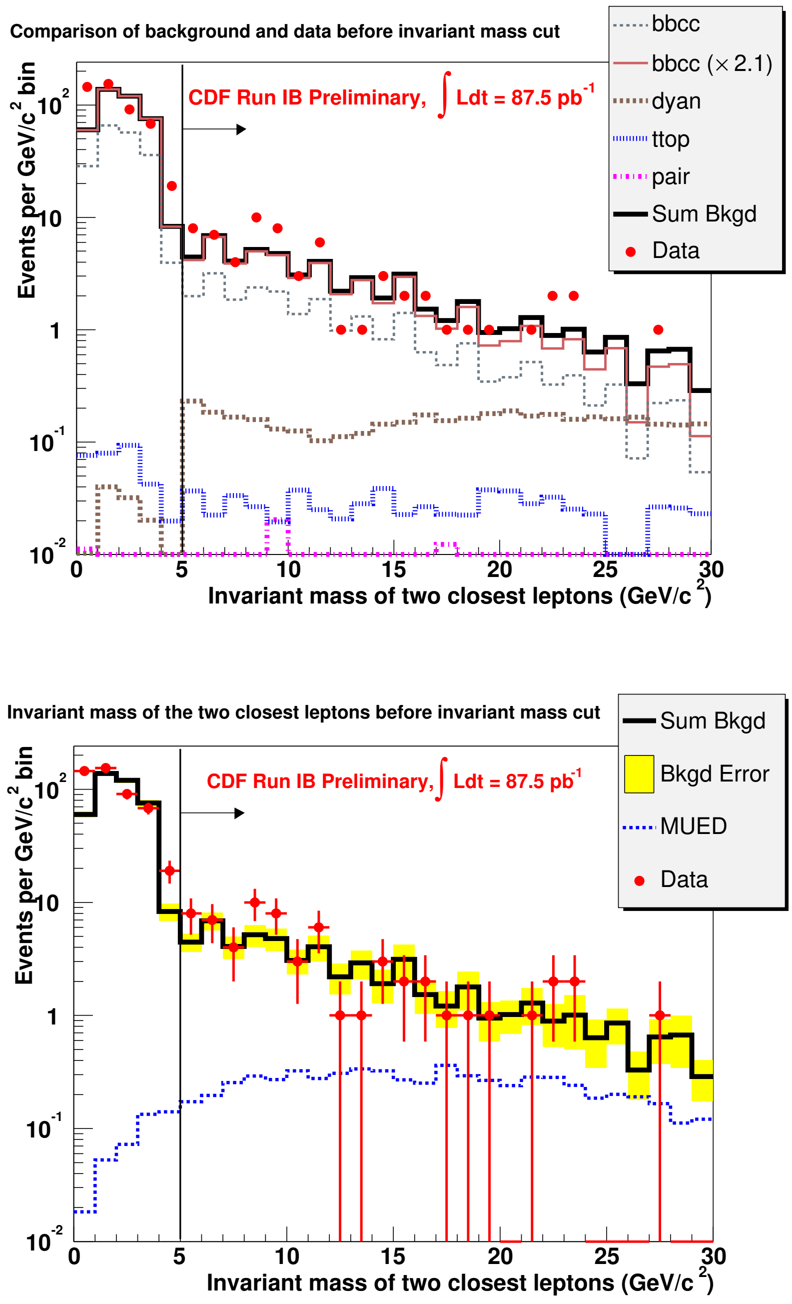

Figure 8: Distributions of invariant mass of the two closest leptons. The top figure shows data and each type of background. The bottom figures shows the MUED signal, data and the total background with error band. The scale factor 2.1 is applied to $b\bar{b}/c\bar{c}$ background, and the total background includes $b\bar{b}/c\bar{c}$ background with scale factor 2.1 applied, Drell-Yan, $t\bar{t}$, and boson pairs. The vertical straight lines indicate the cut value and the arrows indicate the accepted values. Background MC samples are generated by SUSY working group (Appendix D).

6.6 Resonance Removal

So far our data sample still contains e^+e^- or $\mu^+\mu^-$ events that could originate from Z^0 boson or Υ.

These events are removed by an invariant mass cut for the e^+e^- or $\mu^+\mu^-$ pair: $9 \leq m(e^+e^-\ or\ \mu^+\mu^-) \leq 11$ GeV/c^2 for Υ, and $76 \leq m(e^+e^-\ or\ \mu^+\mu^-) \leq 106$ GeV/c^2 for Z^0. An event will be removed if any possible e^+e^- or $\mu^+\mu^-$ pair two-body masses (out of 3 lepton candidates) are in those range.

After resonance removal, we are left with 48 events.

6.7 $\Delta\phi$ Requirements

The Drell-Yan background events from γ^* production and low-p_T Z^0 can be removed with an opening angle cut(see section 4.2). We require the opening angle between the two highest p_T leptons be less than 2.96 radians (170°). See Fig. 9.

After $\Delta\phi$ requirements we are left with 43 events.

6.8 Estimate of Expected Background

Table 10 lists the number of events expected after each cut from each type of background, the sum of all background, the number of data events and a sample MC signal point (R^{-1} = 350 GeV).

6.9 Lepton Candidates Combinations

It is helpful to study the signal MC and the SM background distribution, and examine the three lepton candidates combinations. Fig. 10 and Fig. 11 show the number of events in the eee, $ee\mu$, $e\mu\mu$, $\mu\mu\mu$ channels for the SM background and signal MC respectively and how they change after each cut [18].

After $\Delta\phi$ cut, we have 0.64 signal events and 21.02 total background events in the non-$\mu\mu\mu$ channels (namely eee, $ee\mu$, and $e\mu\mu$), compared with 0.26 signal events and 22.99 total background events in the $\mu\mu\mu$ channel. Clearly the non-$\mu\mu\mu$ channels are better choice for our

[18] All MC events are reconstructed and properly weighted for integrated luminosity, lepton ID efficiency, and trigger efficiency. We add 1 to the number of muons in the Drell-Yan MC events, assuming the fake (third) lepton is most likely a muon.

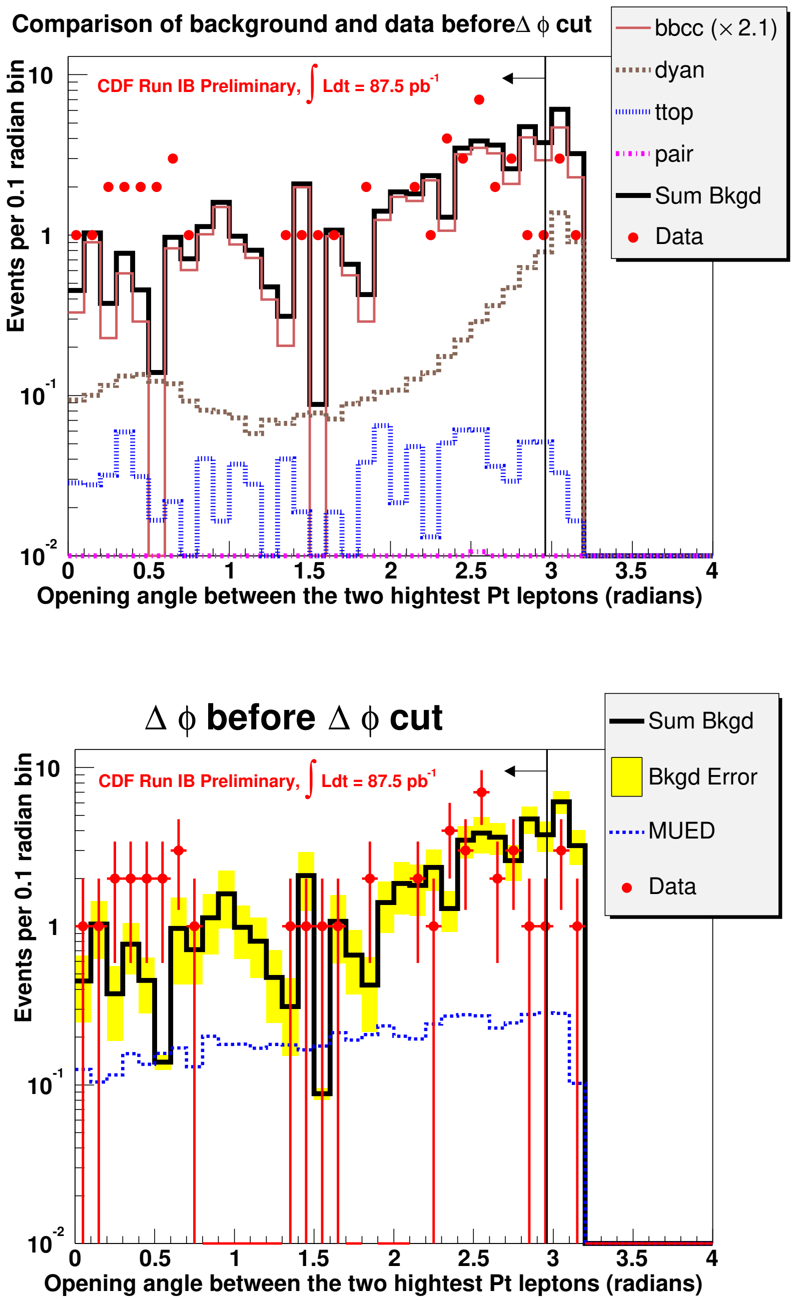

Figure 9: Distributions of opening angle of the two highest transverse momentum leptons. The top figure shows data and each type of background. The bottom figures shows the MUED signal, data and the total background with error band. The scale factor 2.1 is applied to $b\bar{b}/c\bar{c}$ background, and the total background includes $b\bar{b}/c\bar{c}$ background with scale factor 2.1 applied, Drell-Yan, $t\bar{t}$, and boson pairs. The vertical straight lines indicate the cut value and the arrows indicate the accepted values. Background MC samples are generated by SUSY working group (Appendix D).

Table 10: Number of expected background events contributions from $b\bar{b}/c\bar{c}$, Drell-Yan, $t\bar{t}$ and boson pair, total number of expected background, data and signal Monte Carlo events left after each cut. Both background and signal Monte Carlo are weighted by luminosity of 87.5 pb^{-1} , corrected with trigger efficiency, and scaled by the MC correction factor 0.86/event as described in section 5.3.2. An overall scale factor of 2.1 is applied to $b\bar{b}/c\bar{c}$ background. The fake lepton rate 0.0081/event is applied to Drell-Yan background, thus the numbers in the table for Drell-Yan background is the fake lepton rate times the number of dilepton Drell-Yan events.

Cut	Events remaining after each cut $b\bar{b}/c\bar{c}$	Drell-Yan	$t\bar{t}$	Boson Pair	Sum Background	Data	Signal MC ($R^{-1} = 350\ GeV$)
3 lepton requirement	577.58	33.53	2.03	0.40	613.54	1120	1.18
good run requirement	577.58	33.53	2.03	0.40	613.54	1068	1.18
cosmic removal	577.58	33.53	2.03	0.40	613.54	750	1.18
$\lvert z_{vertex}\rvert < 60$ cm	556.23	32.03	1.99	0.38	590.63	725	1.14
Vertex Requirements	555.70	32.03	1.99	0.38	590.10	683	1.14
$\lvert Q_1+Q_2+Q_3\rvert < 3$	539.47	32.03	1.91	0.36	573.77	604	1.14
Require e^+e^- or $\mu^+\mu^-$	454.08	30.72	1.52	0.34	486.66	545	1.10
Invariant Mass > 5 GeV/c^2	52.90	30.61	1.20	0.32	85.03	68	1.02
Z^0 removal (76-106 GeV/c^2)	52.42	7.70	1.04	0.07	61.23	55	1.02
Υ removal (9-11 GeV/c^2)	46.16	7.44	1.02	0.06	54.68	48	0.96
$\Delta\phi_{\ell_1\ell_2} < 170°$	38.14	4.87	0.96	0.05	44.02	43	0.90

analysis. Fig. 12 and Fig. 13 show the invariant mass of two closest leptons and the opening angle of the two highest transverse momentum leptons respectively, in the non-$\mu\mu\mu$ channels.

6.10 Final Optimization Cuts

After all the cuts above are applied, we still have background events remaining. We can further reduce these backgrounds by using isolation[19] and $\not{E}_T$ [20] cuts.

We use the Punzi [29] method to optimize

[19] A lepton's isolation is defined as the energy in a cone of $\Delta R \equiv \sqrt{\Delta\phi^2 + \Delta\eta^2} = 0.4$ minus the electron or muon energy. We require the maximum isolation of the three lepton candidates to be less than our isolation (ISO) cut value. We have considered using the medium or minimum isolation of the three lepton candidates, however the Punzi optimization procedure that we will introduce in this section shows that in order to achieve comparable result as using maximum isolation, the medium or minimum isolation cut has to be less than 1 GeV, which is clearly not a good choice.

[20] $\not{E}_T$ is missing transverse energy. Conservation of energy and momentum allows one to extract the energy and direction of non-interacting particles.

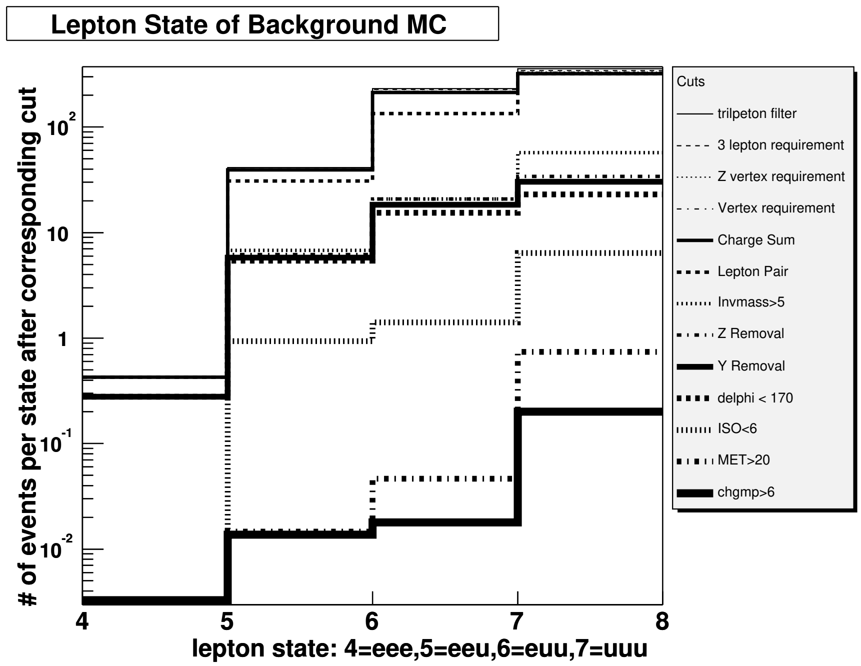

Figure 10: Lepton State Distribution of Reconstructed SM Background MC

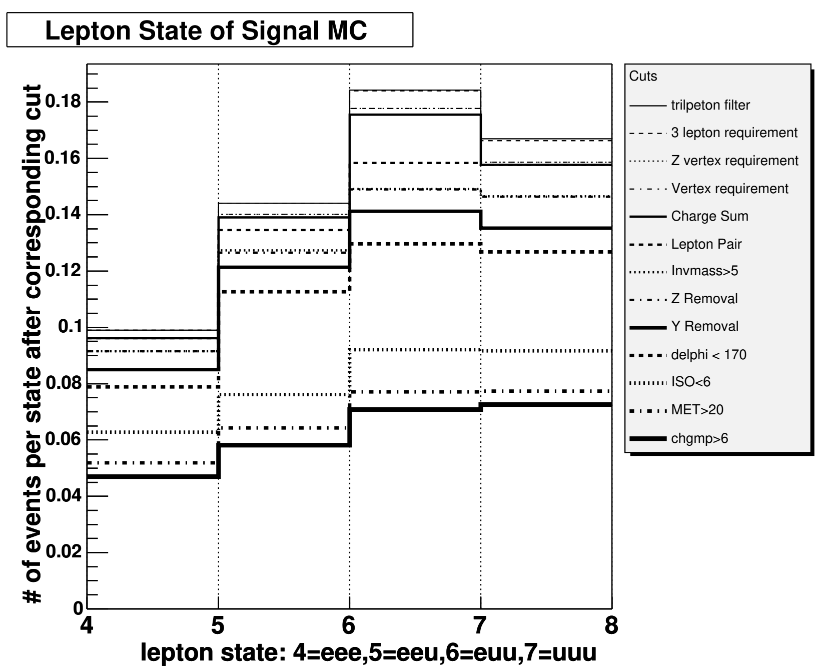

Figure 11: Lepton State Distribution of Reconstructed Signal MC

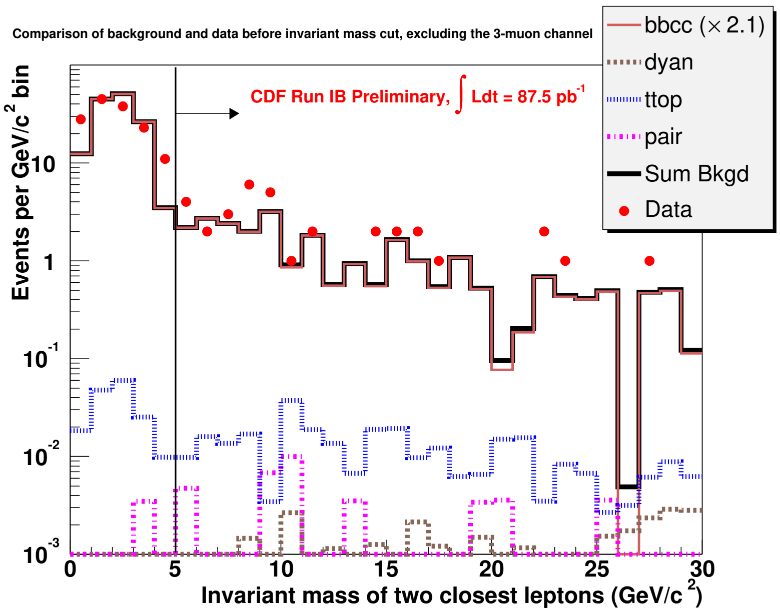

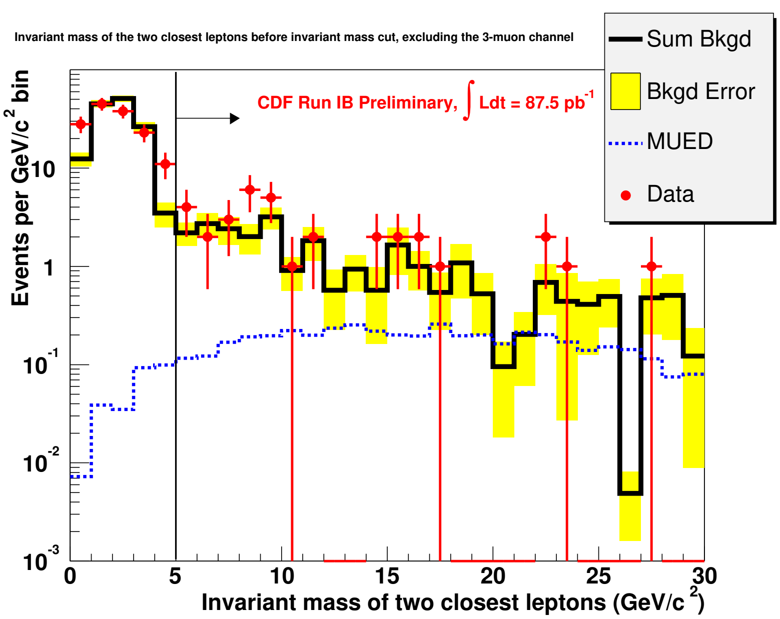

Figure 12: Distributions of invariant mass of the two closest leptons in the non-$\mu\mu\mu$ channels. The top figure shows data and each type of background. The bottom figures shows the MUED signal, data and the total background with error band. The scale factor 2.1 is applied to $b\bar{b}/c\bar{c}$ background, and the total background includes $b\bar{b}/c\bar{c}$ background with scale factor 2.1 applied, Drell-Yan, $t\bar{t}$, and boson pairs. The vertical straight lines indicate the cut value and the arrows indicate the accepted values. Background MC samples are generated by SUSY working group (Appendix D).

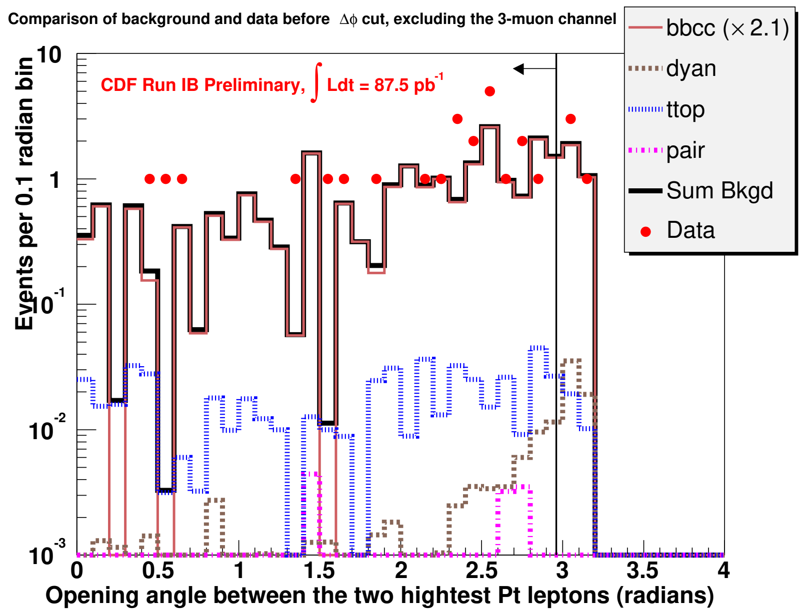

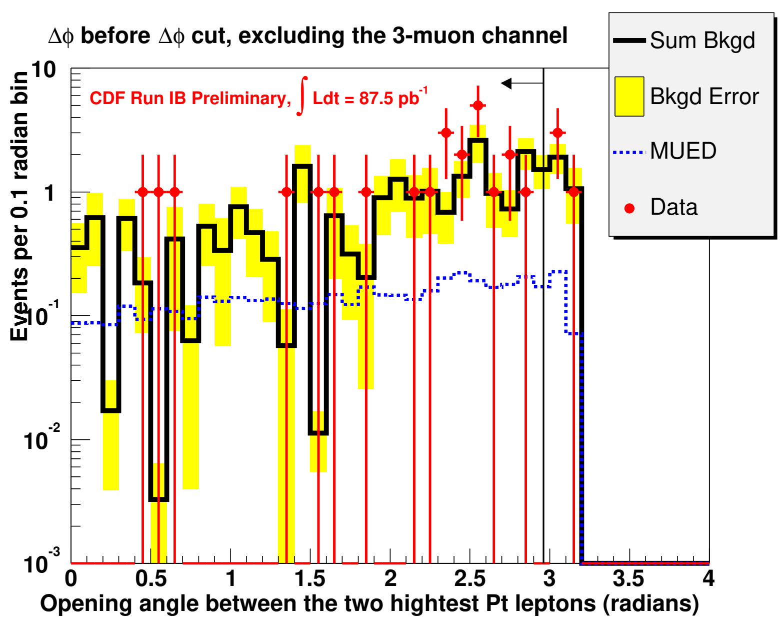

Figure 13: Distributions of opening angle of the two highest transverse momentum leptons in the non-$\mu\mu\mu$ channels. The top figure shows data and each type of background. The bottom figures shows the MUED signal, data and the total background with error band. The scale factor 2.1 is applied to $b\bar{b}/c\bar{c}$ background, and the total background includes $b\bar{b}/c\bar{c}$ background with scale factor 2.1 applied, Drell-Yan, $t\bar{t}$, and boson pairs. The vertical straight lines indicate the cut value and the arrows indicate the accepted values. Background MC samples are generated by SUSY working group (Appendix D).

$$\mathbb{A} \equiv \frac{\epsilon(t)}{a/2 + \sqrt{B(t)}} \tag{11}$$

where t indicates the whole set of cuts, ϵ is the efficiency of the chosen cuts on the signal, a is the number of sigmas corresponding to one-sided Gaussian tests at significance α, and B is the expected number of background events.

$\mathbb{A}$ is independent of the cross section of the new process, thus suitable for searches of new signals and the optimization of the cuts.

We searched a cut matrix with isolation range from 2 GeV to 10 GeV with a step size of 1 GeV, and $\not\!\!E_T$ range from 10 GeV to 30 GeV with a step size of 1 GeV. In Fig. 32, we plot the optimization value $\mathbb{A}$, where $a = 95\%$, with each grid point and charged multiplicity value. We found the following cuts maximize $\mathbb{A}$ for all channels:

$$ISO < 6 \text{ GeV}, \ \not\!\!E_T > 20 \text{ GeV} \tag{12}$$

The number of events expected before and after the final optimization cuts are listed in Appendix H.

Table 11: Optimization grid: rows - Isolation (GeV), columns - $\not\!\!E_T$ (GeV). An integer number is assigned to each combination of isolation and $\not\!\!E_T$ cut, and will be used to denote grid point for the Punzi cut optimization plot Fig. 14. Although we used step size of 1 GeV for isolation and $\not\!\!E_T$ in the actual search, here we use a larger step size for the Table and Figure so they are readable.

Isolation	$\not\!\!E_T$ (GeV)				
(GeV)	10	15	20	25	30
2	1	2	3	4	5
4	6	7	8	9	10
6	11	12	13	14	15
8	16	17	18	19	20
10	21	22	23	24	25

The separate cut optimization for the non-$\mu\mu\mu$ channels and the $\mu\mu\mu$ channel are shown in Fig. 15 and Fig. 16.

We found the following cuts maximize $\mathbb{A}$ for the non-$\mu\mu\mu$ channels:

$$ISO < 4 \text{ GeV}, \ \not\!\!E_T > 15 \text{ GeV} \tag{13}$$

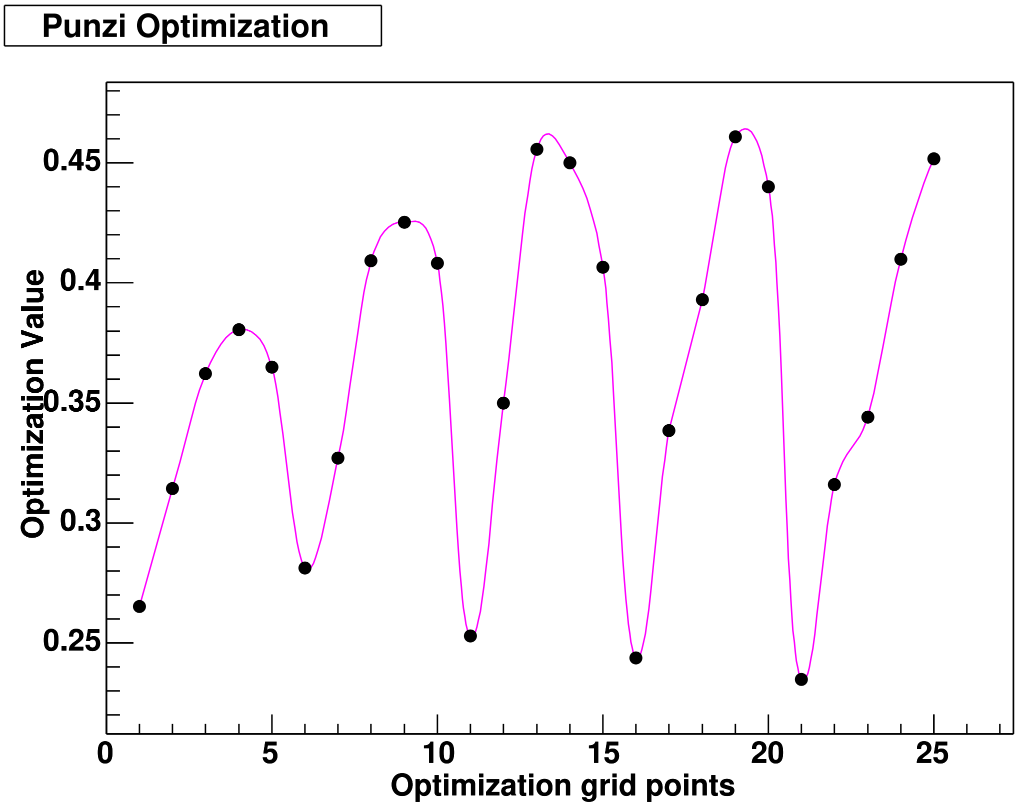

Figure 14: Punzi search of the cut matrix to optimize value $\mathbb{A}$ (y axis), with $a = 95\%$. See Table. 11 for (x axis) grid points.

and the following cuts maximize $\mathbb{A}$ for the $\mu\mu\mu$ channels:

$$ISO < 8 \text{ GeV}, \ \not{E}_T > 20 \text{ GeV} \tag{14}$$

Fig. 17, 18 shows the isolation and $\not{E}_T$ distribution respectively, of the MUED signal Monte Carlo, the SM background, and data, before imposing the final optimization cuts, in the non-$\mu\mu\mu$ channels. Fig. 19 shows $\not{E}_T$ distribution of the MUED signal Monte Carlo, the SM background, and data after the isolation cut in the non-$\mu\mu\mu$ channels.

Table 12 lists the number of events expected before and after the final optimization cuts from each type of background, the sum of all background, the number of data events and a sample MC signal point, separated into non-$\mu\mu\mu$ channels and $\mu\mu\mu$ channel.

The candidate event (Run 63604 Event 108434) in the $\mu\mu\mu$ channel is shown in Appendix I.

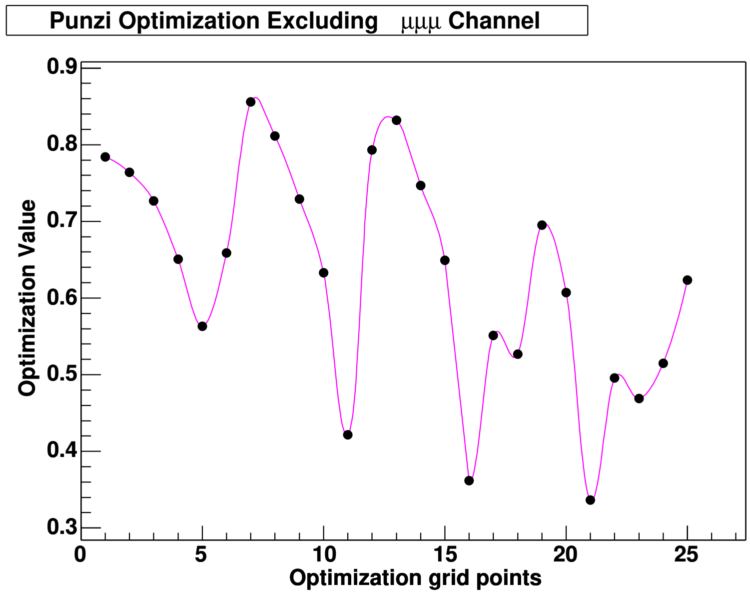

Figure 15: Punzi search in non-$\mu\mu\mu$ channel of the cut matrix to optimize value $\mathbb{A}$ (y axis), with $a = 95\%$. See Table. 11 for (x axis) grid points.

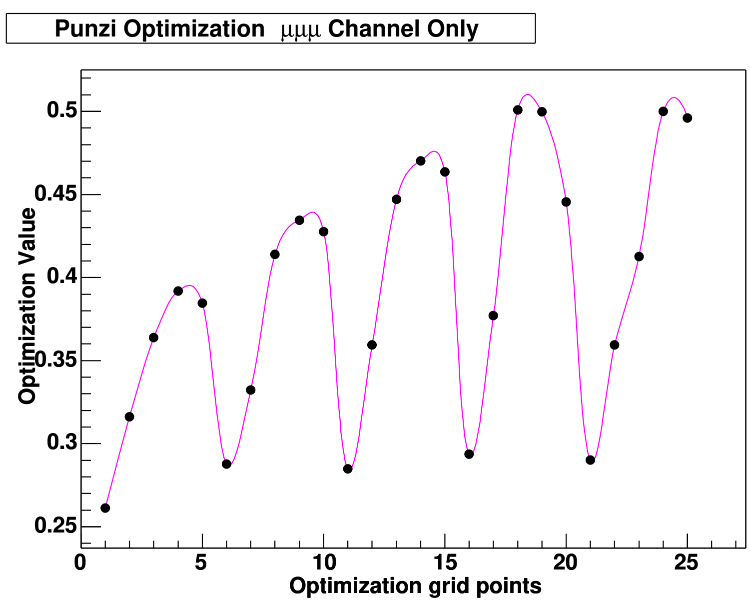

Figure 16: Punzi search in $\mu\mu\mu$ channel of the cut matrix to optimize value $\mathbb{A}$ (y axis), with $a = 95\%$. See Table. 11 for (x axis) grid points.

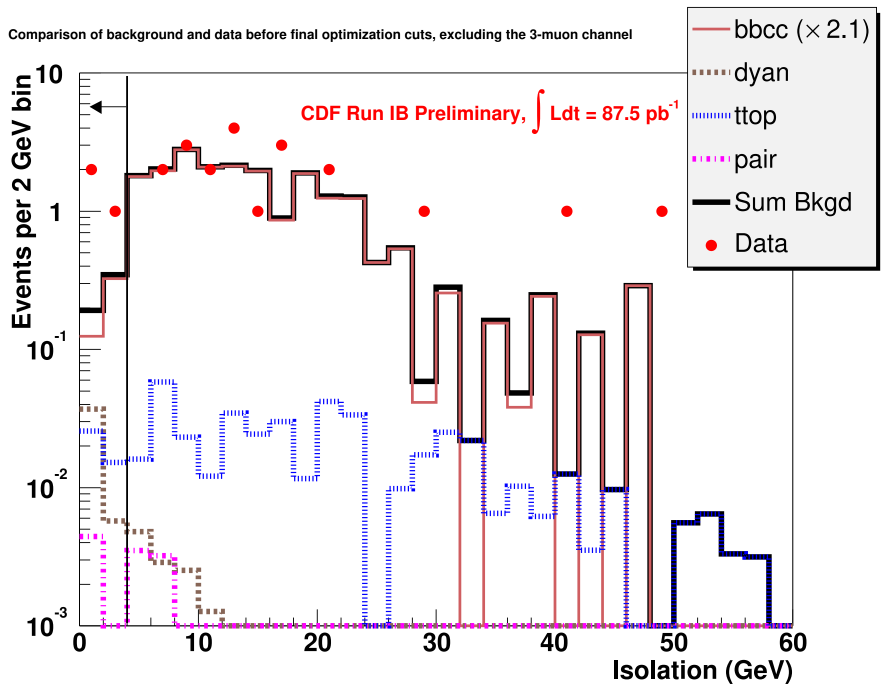

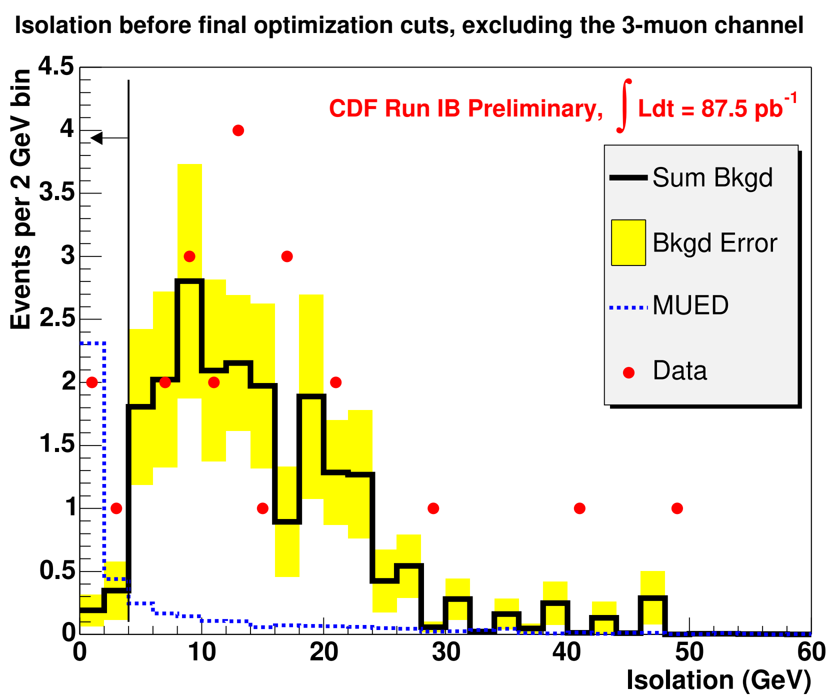

Figure 17: Distributions of isolation in the non-$\mu\mu\mu$ channels. The top figure shows data and each type of background. The bottom figures shows the MUED signal, data and the total background with error band. The scale factor 2.1 is applied to $b\bar{b}/c\bar{c}$ background, and the total background includes $b\bar{b}/c\bar{c}$ background with scale factor 2.1 applied, Drell-Yan, $t\bar{t}$, and boson pairs. The vertical straight lines indicate the cut value and the arrows indicate the accepted values. Background MC samples are generated by SUSY working group (Appendix D).

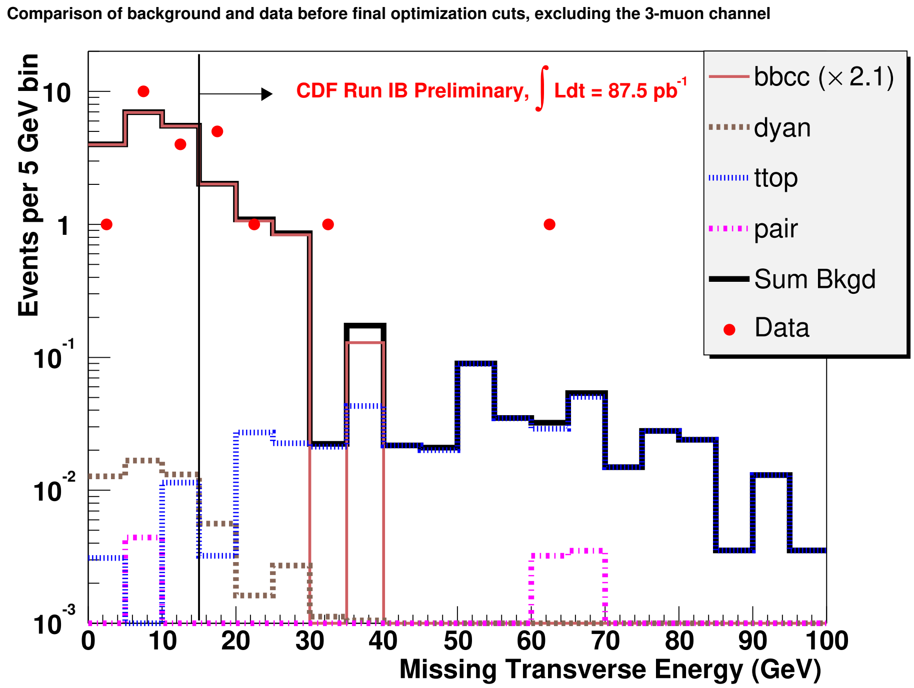

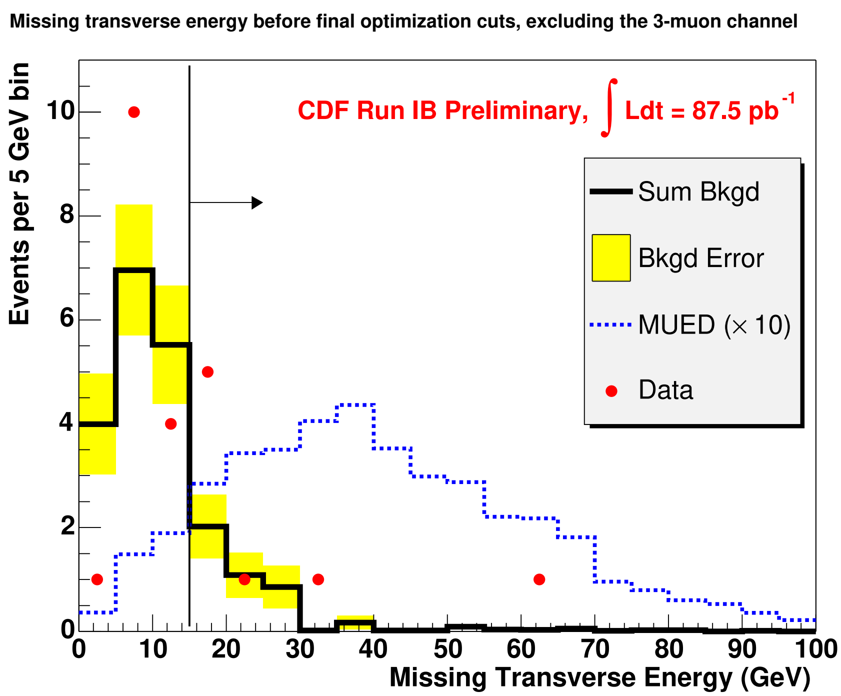

Figure 18: Distributions of missing transverse energy in the non-$\mu\mu\mu$ channels. The top figure shows data and each type of background. The bottom figures shows the MUED signal, data and the total background with error band. The scale factor 2.1 is applied to $b\bar{b}/c\bar{c}$ background, and the total background includes $b\bar{b}/c\bar{c}$ background with scale factor 2.1 applied, Drell-Yan, $t\bar{t}$, and boson pairs. The vertical straight lines indicate the cut value and the arrows indicate the accepted values. Background MC samples are generated by SUSY working group (Appendix D).

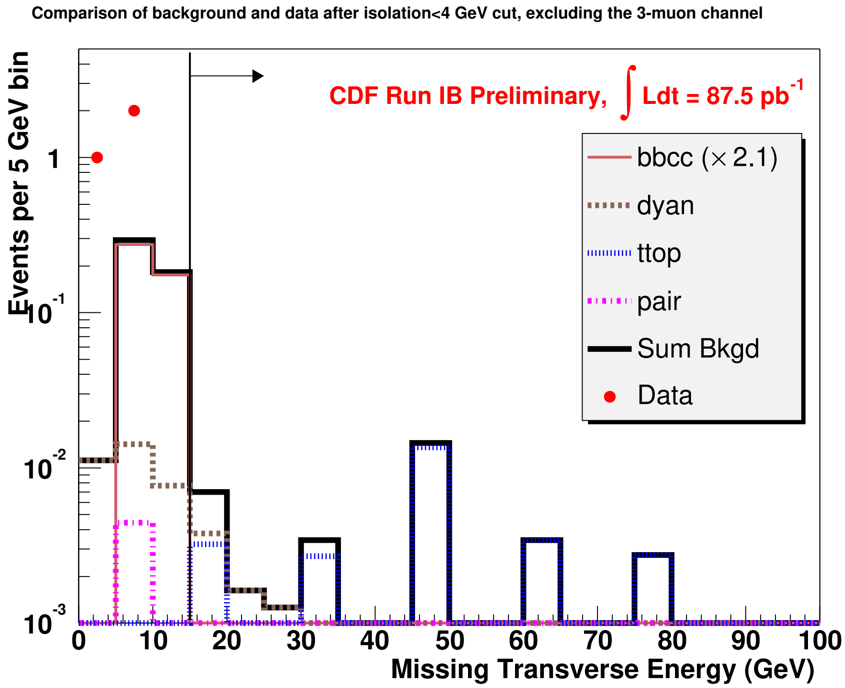

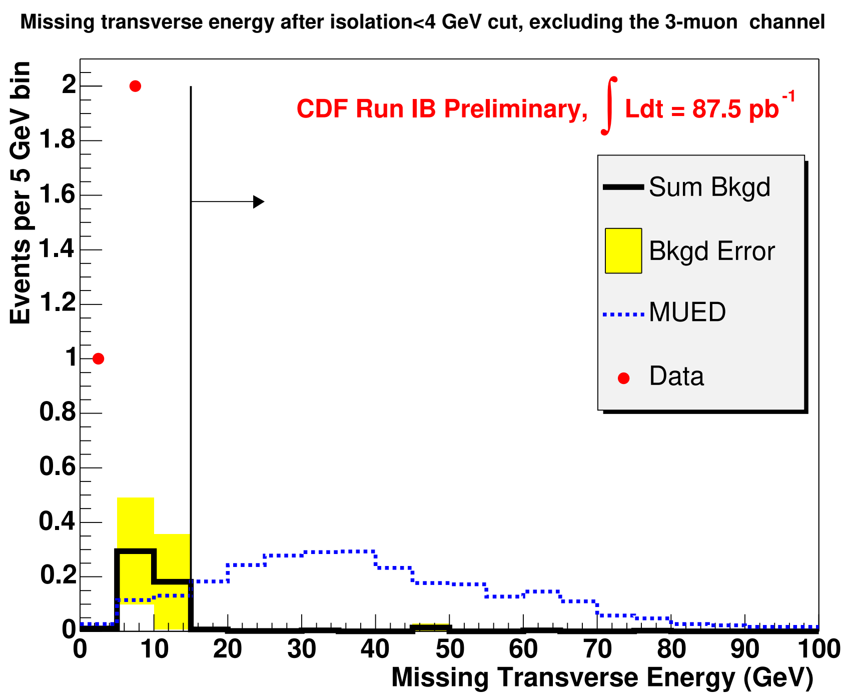

Figure 19: Distributions of missing transverse energy after isolation < 4 GeV cut in the non-$\mu\mu\mu$ channels. The top figure shows data and each type of background. The bottom figures shows the MUED signal, data and the total background with error band. The scale factor 2.1 is applied to $b\bar{b}/c\bar{c}$ background, and the total background includes $b\bar{b}/c\bar{c}$ background with scale factor 2.1 applied, Drell-Yan, $t\bar{t}$, and boson pairs. The vertical straight lines indicate the cut value and the arrows indicate the accepted values. Background MC samples are generated by SUSY working group (Appendix D).

Table 12: Separated into non-$\mu\mu\mu$ channels and $\mu\mu\mu$ channel, number of expected background events contributed by $b\bar{b}/c\bar{c}$, Drell-Yan, $t\bar{t}$ and boson pair production, total number of expected background, data and signal Monte Carlo events remaining after each cut. All MC events are properly weighted with luminosity, lepton ID efficiency, and trigger efficiency.

non-$\mu\mu\mu$ channels	Events remaining after each cut						
	$b\bar{b}/c\bar{c}$	Drell-Yan	$t\bar{t}$	Boson Pair	Sum Background	Data	Signal MC ($R^{-1} = 350\ GeV$)
before final optimization cuts	20.43	0.06	0.52	0.01	21.02	23	0.64
$ISO < 4$ GeV	0.44	0.04	0.04	0.00	0.52	3	0.42
$\not{E}_T > 15$ GeV	0.00	0.01	0.04	0.00	0.05	0	0.38

$\mu\mu\mu$ channel	Events remaining after each cut						
	$b\bar{b}/c\bar{c}$	Drell-Yan	$t\bar{t}$	Boson Pair	Sum Background	Data	Signal MC ($R^{-1} = 350\ GeV$)
before final optimization cuts	17.70	4.81	0.44	0.04	22.99	20	0.26
$ISO < 8$ GeV	1.87	4.71	0.05	0.01	6.64	14	0.20
$\not{E}_T > 20$ GeV	0.00	0.71	0.05	0.00	0.76	1	0.16

7 Limits on UED

In this section we describe the uncertainties relevant to the analysis, the limit setting method and the production cross section limit of the MUED scenario.

7.1 Uncertainties

7.1.1 Systematic Uncertainty

The systematic uncertainty has several components:

- The Run 1B integrated luminosity uncertainty. The uncertainty of the luminosity measurement mainly comes from Beam Beam Counter (BBC) normalization error, because cross sections at CDF are defined with respect to the BBC rate. The reported total uncertainty on the Run 1B integrated luminosity is 4.1% [31]. This uncertainty affects both expected number of signal and background events.

- Trigger efficiency uncertainty. The uncertainty in the trigger efficiency has been studied in the previous trilepton analysis [19]: 5.6%. This uncertainty affects both expected number of signal and background events.

- Lepton identification efficiency uncertainty. Our analysis requires one tight lepton and two loose leptons. The highest uncertainty in lepton identification from Table 7 comes from the tight lepton being a tight central electron (0.98%) and loose leptons being loose CMIO muons(1.54%). Thus overall uncertainty in lepton identification is 3.2% ($\sqrt{(0.98\%)^2 + (1.54\% + 1.54\%)^2}$). This uncertainty affects both expected number of signal and background events.

- Isolation cut efficiency uncertainty. QFL does not simulate lepton isolation correctly due to multiple interactions at high instantaneous luminosity. The highest uncertainty of isolation efficiency at the presence of 2 or more jets is from a muon of 0.904 ± 0.041, which gives us 4.5% uncertainty (see Section 5.3.3). We are picking out the maximum isolation from the three lepton candidates and cutting on that variable. If we can always pick out the correct maximum lepton isolation, then the systematic uncertainty would be 4.5% at most. If we pick the wrong lepton candidate, the isolation uncertainty can only be smaller. So taking 4.5% as the isolation cut efficiency uncertainty is the most conservative approach. This uncertainty affects both expected number of signal and background events.

- Uncertainty from the fake leptons. We used $0.81 \pm 0.07\%$ as the probability that a Drell-Yan dilepton event will have an additional fake lepton (see Section 4.2). The 0.07% error is the statistical error due to the number of leptons used to calculate the fake rate. The relative uncertainty is then 8.6%. In addition, a significant systematic error arises from the definition of a good $W^{\pm}$ event, lepton selection cuts and the use of MC programs, which cannot be easily obtained. We take the total uncertainty of fake leptons as 17.2% by doubling 8.6% as a conservative approach. This uncertainty affects the expected number of background events only.

7.1.2 Statistical Uncertainty

The number of expected MC events $n^{MCexpected}$ (non-integer) is

$$n^{MCexpected} = \sum_{i=1}^{n^{gen}} wgt_i \tag{15}$$

where the integer number n^{gen} is the number of events remaining after all cuts, and wgt_i is the weight of the corresponding event which includes the appropriate luminosity weighting [21] and various efficiency corrections (see Chapter 5.3).

Since events are statistically independent and each event has a weight, wgt_i, the absolute uncertainty of $n^{MCexpected}$ is obtained by summing up each event's weight in quadrature:

$$\Delta n^{MCexpected} = \sqrt{\sum_{i=1}^{n^{gen}} (wgt_i)^2} \tag{16}$$

After final cuts we have 0.54 signal events with absolute uncertainty of 0.014 event, and 0.80 background with absolute uncertainty of 0.018 event. Thus the relative statistical uncertainty of the signal is 2.6% and the relative statistical uncertainty of the background is 2.3%.

7.1.3 Theoretical Uncertainty

The theoretical uncertainty has two components:

- Uncertainty in the structure functions. For the MUED signal Monte Carlo we use the Pythia 6.203 default structure function CTEQ-5L. To study the uncertainty due to this choice, we generated samples with structure function CTEQ-3L and GRV-94L for MC point $R^{-1} = 350$ GeV. After final cuts we have 0.54 signal events (luminosity scaled

[21] We generated large integrated luminosity MC samples and we scale them to the integrated luminosity of the search data sample.

and MC weighted from a final sample size of 1527 events) from CTEQ-5L, 0.53 signal events (luminosity scaled and MC weighted from a final sample size of 1519 events) from CTEQ-3L, and 0.51 signal events (luminosity scaled and MC weighted from a final sample size of 1450 events) from GRV-94L. The average number of events is 0.53 events, and the largest difference between the average and the number from each structure function is 4%. Thus the uncertainty for the expected number of signal events from the structure functions is 4%. For background Monte Carlo generation CTEQ-3L, CTEQ-2L, MRSD0', and GRV-LO structure functions are used, and the uncertainty for the expected number of background events from the structure functions is 7%.

- Uncertainty from initial-state/final-state radiation. For the MUED signal Monte Carlo we enable initial-state and final-state radiation in Pythia generator by default. To study the uncertainty due to this choice, we generated samples with initial-state/final-state radiation turned off, and after final cuts we have 0.52 signal events (luminosity scaled and MC weighted from a final sample size of 1500 events). Comparing with 0.54 signal events (luminosity scaled and MC weighted from a final sample size of 1527 events) with initial-state and final-state radiation on, the average number of events is 0.53 ± 0.01. Thus the uncertainty due to the choice of initial-state/final-state radiation is 2%. This number is applied to MUED signal only.

The uncertainties combine in quadrature for a total signal relative uncertainty of 10.3% [22] and total background relative uncertainty of 20.7% [23].

7.2 Limit Setting Method

The (integer) number of observed events n_0 from an experiment follows a Poisson distribution. If the mean number of events expected is μ (real), then the probability of observing n_0 events is given by

$$P(n_0; \mu) = \frac{\mu^{n_0} e^{-\mu}}{n_0!} \tag{17}$$

In new searches we want to determine a real number N for μ as an upper limit, such that we have probability p to observe n_0 or fewer events. The confidence level is $1 - p$ (the probability to observe more than n_0 events). p can be calculated as

$$p = \sum_{n=0}^{n_0} P(n; N) = \sum_{n=0}^{n_0} \frac{N^n e^{-N}}{n!} \tag{18}$$

[22] $\sqrt{0.041^2 + 0.056^2 + 0.032^2 + 0.045^2 + 0.026^2 + 0.04^2 + 0.02^2} = 10.3\%$

[23] $\sqrt{0.041^2 + 0.056^2 + 0.032^2 + 0.045^2 + 0.172^2 + 0.023^2 + 0.07^2} = 20.7\%$

If we know that μ_B expected background events are among the n_0 observed events, and the number of background events present in the sample is less than or equal to n_0, then we can obtain p as

$$p = \frac{\sum_{n=0}^{n_0} P(n; N + \mu_B)}{\sum_{n=0}^{n_0} P(n; \mu_B)} \tag{19}$$

If the expected number of background events, μ_B, has an uncertainty of σ_B and the expected number of signal events, μ_S, has an uncertainty of σ_S, we can assume they both have Gaussian distributions: $G(\mu_B, \sigma_B) = \frac{1}{\sqrt{2\pi\sigma_B^2}} e^{-\frac{(x-\mu_B)^2}{2\sigma_B^2}}$, $G(\mu_S, \sigma_S) = \frac{1}{\sqrt{2\pi\sigma_S^2}} e^{-\frac{(x-\mu_S)^2}{2\sigma_S^2}}$. We want to determine a real number N for μ_S such that the probability p can be calculated as

$$p = \frac{\sum_{n=0}^{n_0} \frac{1}{\sqrt{2\pi\sigma_N^2}} \int_0^\infty \int_0^\infty P(n; \mu'_B + \mu'_S) e^{-\frac{(\mu_B-\mu'_B)^2}{2\sigma_B^2}} e^{-\frac{(N-\mu'_S)^2}{2\sigma_N^2}} d\mu'_B d\mu'_S}{\sum_{n=0}^{n_0} \int_0^\infty P(n; \mu_B) e^{-\frac{(\mu_B-\mu'_B)^2}{2\sigma_B^2}} d\mu'_B} \tag{20}$$

where $\sigma_N = N\sigma_A/A$ (σ_A is the uncertainty of signal acceptance and A is the signal acceptance), as the relative uncertainty on μ_S comes from the relative uncertainty of the signal acceptance.

The upper limit N can be obtained using various numerical techniques, such as frequentist method and Bayesian method. In this analysis, we obtain the upper limit N on a Poisson process using Bayesian method, which treat the unknown expected number of signal as a random variable with "prior" probability density function $\mathcal{P}(\mu_S)$. Given the observation of n_0 events, a "posterior" probability density function $\mathcal{P}(\mu_S; n_0, \mu_B)$ can be constructed from the likelihood $\mathcal{L}(n_0; \mu_S + \mu_B)$ for observing n_0 events given μ_S expected signal and μ_B expected background.

$$\mathcal{P}(\mu_S; n_0, \mu_B) = \frac{1}{2\pi\sigma_B\sigma_S} \int_0^\infty \int_0^\infty \mathcal{L}(n_0; \mu'_B + \mu'_S) e^{-\frac{(\mu_B-\mu'_B)^2}{2\sigma_B^2}} e^{-\frac{(\mu_S-\mu'_S)^2}{2\sigma_S^2}} d\mu'_B d\mu'_S \tag{21}$$

The upper limit N_{exp} on μ_S can be obtained from p as

$$p = \frac{\int_{N_{exp}}^\infty \mathcal{P}(\mu_S; n_0, \mu_B) d\mu_S}{\int_0^\infty \mathcal{P}(\mu_S; n_0, \mu_B) d\mu_S} \tag{22}$$

For a detailed discussion see [32], and we use program bayes.f in this reference for our calculation.

7.3 Cross Section Limit of KK Q_1Q_1 Pair Production

The total signal relative uncertainty is 10.3% and the total background relative uncertainty is 20.7%.

Having observed 0 events with 0.05 expected background events in the non-$\mu\mu\mu$ channels, we obtain $N_{exp} = 3.08$ (2.36) at Confidence Level of 95% (90%). [24]

Having observed 1 event with 0.76 expected background events in the $\mu\mu\mu$ channel, we obtain $N_{exp} = 4.36$ (3.48) at Confidence Level of 95% (90%). [25]

We use the formula

$$\sigma_{Q_1Q_1} \cdot \mathrm{BR}(Q_1Q_1 \to lll + X) \quad < \quad \frac{N_{exp}}{\epsilon^{tot} \cdot \displaystyle\int \mathcal{L}dt} \tag{23}$$

to set the upper limit for Q_1Q_1 production cross section times the branching ratio to trilepton [26] final states with the number of expected events divided by the detection efficiency times the integrated luminosity.

The detection efficiency is the combination of geometric acceptance, kinematic acceptance and trigger efficiency. At signal MC point ($R^{-1} = 350$ GeV, $\Lambda R = 20$, Higgs mass $m_h = 120$ GeV) we started with 25,000 events. After trilepton analysis selection (see section 3.3) we have 3391 events, thus $\epsilon_1 = 13.6\%$. After final cuts (with trigger efficiency factor, lepton ID efficiency factor and isolation efficiency factor applied) we have 1247.0 events (879.8 events in the non-$\mu\mu\mu$ channels and 374.7 events in the $\mu\mu\mu$ channel), thus $\epsilon_2 = 36.8\%$. The total detection efficiency is thus $\epsilon^{tot} = 5.0\%$ (3.5% for the non-$\mu\mu\mu$ channels and 1.5% for the $\mu\mu\mu$ channel).

We used b quark flavor when generating our signal MC sample, and there are total of 5 flavors excluding top quark. In order to compare with other quark flavors, we generated signal MC sample using u quark at $R^{-1} = 350$ GeV and obtained $\epsilon^{tot} = 4.9\%$ (3.5% for the non-$\mu\mu\mu$ channels and 1.4% for the $\mu\mu\mu$ channel). The difference of total detection efficiency

[24] If we use charged multiplicity cut, we would observe 0 events with 0.02 expected background events, thus $N_{exp} = 3.08$ (2.36) at Confidence Level of 95% (90%).

[25] If we use charged multiplicity cut, we would observe 1 event with 0.21 expected background events, thus $N_{exp} = 4.66$ (3.77) at Confidence Level of 95% (90%).

[26] Here we only consider electrons and muons

using different quark flavors is less than 2%. We take the average value 3.5% for the non-$\mu\mu\mu$ channels and 1.45% for the $\mu\mu\mu$ channel as the detection efficiency.

From Table 1, we obtain $\mathrm{BR}(Q_1 Q_1 \to lll + X) = \frac{5}{9} \times \frac{5}{9} = \frac{25}{81}$. Run 1B $\int \mathcal{L} dt = 87.5\ \mathrm{pb}^{-1}$.

At signal MC point ($R^{-1} = 350$ GeV, $\Lambda R = 20$, Higgs mass $m_h = 120$ GeV), the non-$\mu\mu\mu$ channels $Q_1 Q_1$ production cross section limit at Confidence Level of 95% (90%) is:

$$\sigma_{Q_1 Q_1} \quad < 3.3 \text{ pb } (2.5 \text{ pb}) \; ; \tag{24}$$

$Q_1 Q_1$ production cross section is $\frac{1}{2}$ total KK quark production cross section (see section 2.3), thus the non-$\mu\mu\mu$ channels KK quark (excluding KK top) production cross section limit at Confidence Level of 95% (90%) is 6.6 pb (5.0 pb). Converting it to an extra dimension radius limit according to Fig. 6 we have $R^{-1} >$ 270 GeV (280 GeV).

The $\mu\mu\mu$ channel $Q_1 Q_1$ production cross section limit at Confidence Level of 95% (90%) is:

$$\sigma_{Q_1 Q_1} \quad < 11.1 \text{ pb } (8.9 \text{ pb}) \; ; \tag{25}$$

Thus the $\mu\mu\mu$ channel KK quark (excluding KK top) production cross section limit at Confidence Level of 95% (90%) is 22.2 pb (17.8 pb). Converting it to an extra dimension radius limit according to Fig. 6 we have $R^{-1} >$ 230 GeV (240 GeV).

7.4 Cross Section Limit of KK Quark Pair Production + KK Gluon-Quark Production + KK Gluon Pair Production

Till now we only considered KK quark pairs production since they have the largest cross section among all KK states (see Fig. 6). If we consider KK gluon-quark production and KK gluon pair production, equation (23) would become:

$$\begin{aligned} N_{exp} > (&\epsilon_{Q_1 Q_1} \cdot \sigma_{\text{KK quark pair}} \cdot \mathrm{BR}(\text{KK quark pair} \to lll + X) + \\ &\epsilon_{g_1 Q_1} \cdot \sigma_{\text{KK gluon}-\text{quark}} \cdot \mathrm{BR}(\text{KK gluon} - \text{quark} \to lll + X) + \\ &\epsilon_{g_1 g_1} \cdot \sigma_{\text{KK quark pair}} \cdot \mathrm{BR}(\text{KK quark pair} \to lll + X)) \\ &\cdot \int \mathcal{L} dt \end{aligned}$$

We generated KK gluon-quark sample and KK gluon pair sample at 350 GeV. Using the same cuts as we did for KK quark pairs, we obtained the total detection efficiency for the KK gluon-quark and KK gluon pair samples listed in Table 13:

What we care about is how many SU(2)-doublet KK quarks are produced:

Table 13: Total Detection Efficiency (non-$\mu\mu\mu$, $\mu\mu\mu$)

Sample	Total Detection Efficiency
Q_1Q_1	5.0% (3.5%, 1.5%)
g_1Q_1	3.0% (2.1%, 0.9%)
g_1g_1	3.0% (2.0%, 1.0%)

- 1/2 of the $n = 1$ mode KK quark pairs are Q_1Q_1 (if we ignore the small mass splitting between doublets and singlets).

- 1/2 of the $n = 1$ mode KK gluon-quark produced are g_1Q_1, and 1/2 of the KK g_1 decay to Q_1Q_0, so overall 1/4 of the KK gluon-quark contribute three or four leptons.

- 1/4 of the $n = 1$ mode KK gluon pairs would decay to $Q_1Q_0Q_1Q_0$

At 350 GeV, the production cross section for KK quark pairs, gluon-quark, gluon pairs are 0.7 pb, 0.15 pb, and 0.08 pb respectively(see Fig. 6) [27], thus $\sigma_{\text{KK gluon-quark}} = 0.21\sigma_{\text{KK quark pair}}$, $\sigma_{\text{KK quark pair}} = 0.11\sigma_{\text{KK quark pair}}$.

For the non-$\mu\mu\mu$ channels we have:

$$\begin{aligned} N_{exp} = (0.035 \times \sigma_{\text{KK quark pair}} \times \frac{1}{2} \times \text{BR}(Q_1Q_1 \to lll + X) + \\ 0.021 \times 0.21 \times \sigma_{\text{KK quark pair}} \times \frac{1}{4} \times \text{BR}(Q_1Q_1 \to lll + X) + \\ 0.020 \times 0.11 \times \sigma_{\text{KK quark pair}} \times \frac{1}{4} \times \text{BR}(Q_1Q_1 \to lll + X)) \\ \cdot \int \mathcal{L}dt \end{aligned}$$

We obtain $\sigma_{\text{KK quark pair}} < 6.0$ pb (4.6 pb) at Confidence Level of 95% (90%)

Ignore KK top production,

$\sigma_{tot} = \sigma_{\text{KK quark pair}} + \sigma_{\text{KK gluon-quark}} + \sigma_{\text{KK gluon pair}} < 7.9$ pb (6.0 pb)

Converting it to an extra dimension radius limit according to Fig. 6 we have $R^{-1} >$ 280 GeV (290 GeV).

[27] The production cross section relevant for the trilepton signal is 1/2 * 0.7 + 1/4 * 0.15 + 1/4 * 0.08 = 0.4075 pb.

For the $\mu\mu\mu$ channel we have:

$$\begin{aligned} N_{exp} = (0.0145 \times \sigma_{\text{KK quark pair}} \times \frac{1}{2} \times \text{BR}(Q_1Q_1 \to lll + X) + \\ 0.009 \times 0.21 \times \sigma_{\text{KK quark pair}} \times \frac{1}{4} \times \text{BR}(Q_1Q_1 \to lll + X) + \\ 0.010 \times 0.11 \times \sigma_{\text{KK quark pair}} \times \frac{1}{4} \times \text{BR}(Q_1Q_1 \to lll + X)) \\ \cdot \int \mathcal{L}dt \end{aligned}$$

We obtain $\sigma_{\text{KK quark pair}} < 22.3$ pb (18.0 pb) at Confidence Level of 95% (90%)

Ignore KK top production,

$\sigma_{tot} < 29.4$ pb (23.8 pb)

Converting it to an extra dimension radius limit according to Fig. 6 we have $R^{-1} >$ 240 GeV (250 GeV).

7.5 Conclusion

We have searched for Univeral Extra Dimension using CDF run I data at Fermilab Tevatron and set a limit for the KK quark production cross section. More data has been collected in CDF Run II, and an analysis in Run II can be done using the same analysis technique once the SM background samples are in place.

References

[1] T. Appelquist, H.-C. Cheng and B. A. Dobrescu, *Bounds on Universal Extra Dimensions*, Phys. Rev. D **64**, 035002 (2001), hep-ph/0012100.

[2] T. Kaluza, Sitzungsber. Preuss. Akad. Wiss., Phys. Math. Klasse (1921) 966.

[3] O. Klein, Nature **188** (1926) 516.

[4] C. Macesanu, C. D. McMullen and S. Nandi, *Collider Implications of Universal Extra Dimensions*, Phys. Rev. D **66**, 015009 (2002), hep-ph/0201300.

[5] D. A. Dicus, C. D. McMullen and S. Nandi, *Collider Implications of Kaluza-Klein Excitations of the Gluons*, Phys. Rev. D **65**, 076007 (2002), hep-ph/0012259.

[6] H.-C. Cheng, K. T. Matchev and M. Schmaltz, *Radiative Corrections to Kaluza-Klein Masses*, Phys. Rev. D **66**, 036005 (2002), hep-ph/0204342.

[7] C. D. Carone, J. M. Conroy, M. Sher, and I. Turan, *Universal Extra Dimensions and Kaluza Klein Bound States*, Phys. Rev. D **69**, 074018 (2004), hep-ph/0312055.

[8] T. G. Rizzo, *Probes of Universal Extra Dimensions at Colliders*, Phys. Rev. D **64**, 095010 (2001), hep-ph/0106336.

[9] H.-C. Cheng, K. T. Matchev and M. Schmaltz, *Bosonic Supersymmetry? Getting Fooled at the LHC*, Phys. Rev. D **66**, 056006 (2002), hep-ph/0205314.

[10] F. Abe, *et al.*, (The CDF Collaboration), Phys. Rev. **D50**, 2966 (1994); D. Amidei, *et al.*, Nucl. Instrum. Methods **A350**, 73 (1994)

[11] F. Abe, *et al.*, (The CDF Collaboration), *Search for Chargino-Neutralino Production at the Fermilab Tevatron Collider*, Phys. Rev. Lett. **80**, 5275 (1998).

[12] E. Buckley-Geer and S. Lammel, *How to Find Out What Run 1B Data is Available*, CDF Note 2657 (1995).

[13] J.P. Done et al.,*SUSY Dilepton Selection for Run I*, CDF Note 4446 (1998). Also see CDF Note 3472.

[14] T. Abe et al., The CDF Collaboration, *Measurement of the B Meson and b Quark Cross Section at sqrts = 1.8 TeV Using the Exclusive Decay B0 –¿ J/psi K*(892)0*, Phys. Rev. D **50**, 4252 (1994).

Todd. A. Keaffaber, *Measurement of the B+ Meson Cross Section in Proton-Antiproton Collisions at 1.8 TeV*, CDF Note 5443 (2000).

[15] T. Affolder et al., The CDF Collaboration, *Measurement of the tt-bar Production Cross Section in p anti-p Collisions at s**(1/2) = 1.8 TeV*, Phys. Rev. D **64**, 032002 (2001).

[16] J. Ohnemus, J. F. Owens *Order- alpha_s calculation of hadronic ZZ production*, Phys. Rev. D **43**, 3626 (1991); J. Ohnemus, *Order- alpha_s calculation of hadronic WZ production*, Phys. Rev. D **44**, 3477 (1991); J. Ohnemus, *Order- alpha_s calculation of hadronic W-W+ production*, Phys. Rev. D **44**, 1403 (1991).

J. M. Campbell, R. K. Ellis *An update on vector boson pair production at hadron colliders*, Phys. Rev. D **60**, 113006 (1999), hep-ph/9905386.

[17] F. Abe et al., The CDF Collaboration, *Measurement of Z0 and Drell-Yan production cross sections using dimuons in p-barp collisions at sqrt[s]=1.8 TeV*, Phys. Rev. D **59**, 052002 (1999).

[18] F. Abe et al., The CDF Collaboration, *Measurement of Drell-Yan electron and muon pair differential cross sections in p-barp collisions at sqrt[s]=1.8 TeV*, Phys. Rev. D **49**, 1 (1994).

[19] B. Tannenbaum, *A Search for Chargino-Neutralino Production at the Fermilab Tevatron Collider*, CDF Note 4571 (1998).

[20] S. Tether, *The Fake Lepton Rate for the Run 1B Susy Trilepton Analysis*, CDF Note 3566 (1996).

[21] H. Baer, F.E. Paige, S.D. Protopescu, X. Tata, *ISAJET 7.40: A Monte Carlo Event Generator for* $pp, \bar{p}p$, *and* e^+e^- *Reactions*, hep-ph/9810440 (1998).

[22] T. Sjostrand, L. Lonnblad, S. Mrenna, *PYTHIA 6.2 Physics and Manual*, hep-ph/0108264 (2001).

[23] M. SHAPIRO et al, *A User's Guide to QFL*, CDF Note 1810 (1992).

[24] J.P. Done, M. Chertok, T. Kamon, *Study of Run 1B Lepton Identification Efficiencies for SUSY searches*, CDF Note 4218 (1997).

[25] J.P. Done, M. Chertok, T. Kamon, *Study of Run-1B Lepton Isolation Efficiencies for SUSY Searches*, CDF Note 4291 (1997).

[26] S. Kopp and C. Grosso-Pilcher, *A Good Run List for The 1992-1993 CDF Run*, CDF Note 1992 (1993).

[27] M. Krasberg, T. LeCompte, *CMCOS: The Run 1A Cosmic Ray Filter*, CDF Note 2032 (1993).

[28] A. Koen, *Search for R-Parity Violating Susy in the CDF Multi-Lepton Channel*, CDF Note 5212 (1999).

[29] G. Punzi, *Sensitivity of Searches for New Signals and its Optimization* hep-physics/0308063.

[30] A. Korytov, A. Pronko, A. Safonov, *Update on the measurement of charged particle multiplicities in gluon and quark jets*, CDF Note 6809,5899 (2003).

[31] D. Cronin-Hennessy, A. Beretvas, *Luminosity at CDF*, CDF Note 4721 (1998).

[32] J. Conway, K. Maeshima, *Upper Limits on Poisson Processes Incorporating Uncertainties in Acceptance and Background*, CDF Note 4476 (1998).

A MUED Radiative Corrections to Kaluza-Klein Masses

The radiative corrections to the KK spectrum were calculated by Cheng, Matchev and Schmaltz [6] using the one-loop leading log approximation. The corrections to the masses of the KK modes contains both bulk terms and boundary terms.

The bulk corrections are:

$$
\begin{aligned}
\delta\left(m_{B_n}^2\right) &= -\frac{39}{2}\,\frac{g'^2\,\zeta(3)}{16\pi^4}\left(\frac{1}{R}\right)^2, \\
\delta\left(m_{W_n}^2\right) &= -\frac{5}{2}\,\frac{g_2^2\,\zeta(3)}{16\pi^4}\left(\frac{1}{R}\right)^2, \\
\delta\left(m_{g_n}^2\right) &= -\frac{3}{2}\,\frac{g_3^2\,\zeta(3)}{16\pi^4}\left(\frac{1}{R}\right)^2, \\
\delta(m_{f_n}) &= 0, \\
\delta(m_{H_n}^2) &= 0
\end{aligned} \tag{26}
$$

The boundary corrections are:

$$
\begin{aligned}
\bar{\delta}\left(m_{B_n}^2\right) &= m_n^2\left(-\frac{1}{6}\right)\frac{g'^2}{16\pi^2}\ln\frac{\Lambda^2}{\mu^2}, \\
\bar{\delta}\left(m_{W_n}^2\right) &= m_n^2\,\frac{15}{2}\,\frac{g_2^2}{16\pi^2}\ln\frac{\Lambda^2}{\mu^2}, \\
\bar{\delta}\left(m_{g_n}^2\right) &= m_n^2\,\frac{23}{2}\,\frac{g_3^2}{16\pi^2}\ln\frac{\Lambda^2}{\mu^2}, \\
\bar{\delta}\,m_{Q_n} &= m_n\left(3\,\frac{g_3^2}{16\pi^2}+\frac{27}{16}\,\frac{g_2^2}{16\pi^2}+\frac{1}{16}\,\frac{g'^2}{16\pi^2}\right)\ln\frac{\Lambda^2}{\mu^2}, \\
\bar{\delta}\,m_{L_n} &= m_n\left(\frac{27}{16}\,\frac{g_2^2}{16\pi^2}+\frac{9}{16}\,\frac{g'^2}{16\pi^2}\right)\ln\frac{\Lambda^2}{\mu^2}\,.
\end{aligned} \tag{27}
$$

Here B_n are the KK $U(1)$ hypercharge gauge bosons, W_n are the KK $SU(2)_W$ gauge bosons, g_n are the KK gluons, Q_n are the KK $SU(2)$-doublet quarks, and L_n are the KK $SU(2)$-doublet leptons. The renormalization scale μ should be taken to be approximately the mass of the corresponding KK mode. g_3, g_2, g' are $SU(3)_C$, $SU(2)_L$, and $U(1)_Y$ couplings respectively: $\alpha_s = g_3^2/4\pi$, $\alpha_{EM} = e^2/4\pi$, $e = g_2 \sin\theta_{\rm W}$, $\sin^2\theta_{\rm W} = ({\rm g'})^2/({\rm g}_2^2 + ({\rm g'})^2)$.

B Lepton Identification Cuts

B.1 Electron identification cuts

The electrons are identified by using calorimeters and the associated track measured in the CTC.

$\mathrm{p_T}$ is the transverse momentum of the track associated with the electron candidate measured in the CTC. A $\mathrm{p_T}$ cut is applied only to CEM electron candidates since PEM electrons will not travel through the entire CTC thus their $\mathrm{p_T}$ measurement is not accurate.

E_T is the transverse energy of the electromagnetic calorimeter cluster associated with the electron candidate.

E/p is the ratio of the electron candidate's energy to its momentum. The electron candidate of interest has energies in the GeV scale thus its momentum is roughly the same as its energy. The $E/p < 2$ requirement assures that the electron energy and its momentum agree and allows rejection of photons from π^0 decays. E/p cut is not applied to PEM electrons.

E_{HAD}/E_{EM} is the ratio of the hadronic energy to the electromagnetic energy associated with the cluster. For electrons, most of the energy is deposited in the electromagnetic calorimeter so we require $E_{HAD}/E_{EM} \leqslant 0.05$ for a tight electron, $E_{HAD}/E_{EM} \leqslant 0.055 + 0.045 \times \frac{E}{100}$ for a loose CEM and $E_{HAD}/E_{EM} \leqslant 0.1$ for a loose PEM. The sliding cut for loose CEM electrons allows electron candidates to have greater average energy leakage with higher energies. The constant term dominates for low energy electrons and the cut is always looser than the fixed cut used for the tight electron.

L_{SHR} is the lateral shower profile of the electromagnetic shower. To take into account the fact that electron showers sometimes spread over more than one electromagnetic tower, we define variable L_{SHR} to be

$$L_{SHR} \equiv 0.14 \sum_i \frac{E_i^{\mathrm{adj}} - E_i^{\mathrm{prob}}}{\sqrt{0.14^2 E + (\Delta E_i^{\mathrm{prob}})^2}}$$

where E_i^{adj} and E_i^{prob} are the measured and expected energy in a tower adjacent to the seed tower, $0.14\sqrt{E}$ is the uncertainty of the energy measurement, $\Delta E_i^{\mathrm{prob}}$ the uncertainty of the energy estimate, E_i^{prob} is calculated using a parameterization from test beam data, and the sum goes over all towers in the electromagnetic cluster. All energies are measured in GeV. Hadrons generally have different shower profile from electrons, and thus are rejected by this cut. L_{SHR} cut is not applied to PEM electrons.

$|\Delta x|$ **and** $|\Delta z|$ are the track to shower matching variables. An alignment corrected CTC track is extrapolated to the Central Electromagnetic Strip chambers (CES) and compared with the shower position. $|\Delta x|$ is the matching in the $r - \phi$ plane and $|\Delta z|$ is the matching in the z direction. Background from overlapping neutral or charged hadrons can be rejected by requiring a good matching. This cut is not applied to PEM electrons.

χ^2_{strip} is the strip chamber profile comparison variable. It is a fit of the energy deposited in the CES strips using the 11 strips in z-direction per CES chamber to the profile determined during the test beam. χ^2_{strip} cut ensures that the electron candidate exhibits the same characteristics as its test beam counterpart. This cut is not applied to PEM candidates.

$\chi^2_{3\times3}$ is a fit of the lateral sharing of energy in the three towers in η by the three towers in ϕ around the electron cluster's center to the profile determined during the test beam. This cut is applied only to PEM electrons.

VTX occupancy is the ratio of layers in the VTX where the electron deposits energy to the number of layers where the electron should deposit energy according to its trajectory. We use this cut to ensure the presence of a charged track, thus reject photons from the PEM electron candidates. VTX occupancy cut is only applied to PEM candidates.

B.2 Muon Identification Cuts

The muon identification cuts are based on information obtained from the CTC and the muon chambers. The calorimeter data is also used for verification of a minimal ionizing particle passing through the detector.

$\mathrm{p_T}$ is the transverse momentum of the track associated with the muon candidate as measured by the CTC. Note that the CMIO cut is 10 GeV/c since the bank is created only for tracks with $\mathrm{p_T}$ above 10 GeV/c.

E_{EM}, E_{HAD} is the energy deposited in the electromagnetic and hadronic calorimeters respectively. A high $\mathrm{p_T}$ muon will not deposit substantial amounts of energy in any calorimeter. The hadronic calorimeters contain more absorber material than the electromagnetic calorimeters so a muon could deposit more energy in hadronic calorimeters than electromagnetic calorimeters.

d_0 **raw** is the impact parameter, *i.e.* the distance of the closest approach of the reconstructed track to the beam line. It requires the muon to originate from near the nominal interaction region. This cut mainly rejects cosmic muons in the sample.

Matching requires a good match between the extrapolation of the CTC track and the muon chamber stubs. We require that either the $r - \phi$ distance between the extrapolation ($|\Delta x|$) be less than a certain value or the χ^2_x of a fit from the CTC track to the muon stub be less than 9.0. This cut is not applied to CMIO muons.

C MUED Signal Monte Carlo Simulations

All plots in this appendix are from MUED signal at R^{-1}=350 GeV.

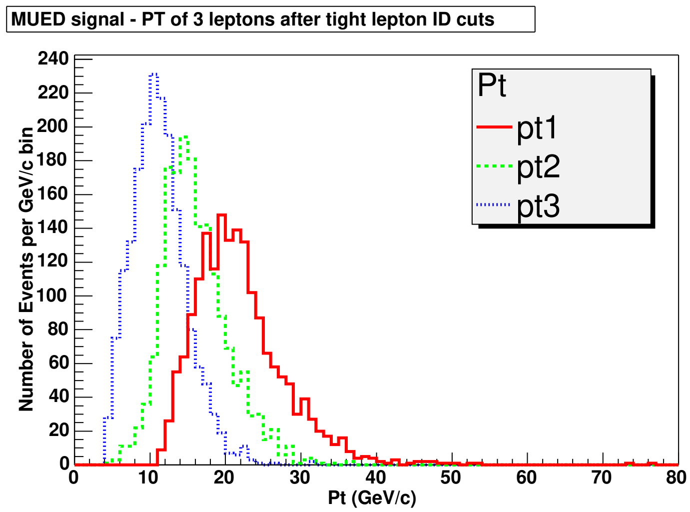

Figure 20: MUED signal MC transverse momentum of three leptons after tight lepton cuts (as described in section 3.3). pt1, pt2, pt3 are the transverse momenta of the three leptons from the highest to the lowest transverse momentum respectively.

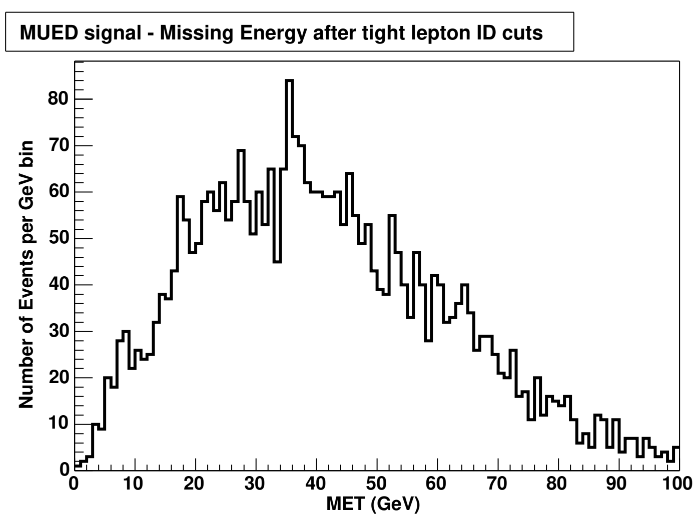

Figure 21: MUED signal MC missing energy after tight lepton cuts (as described in section 3.3).

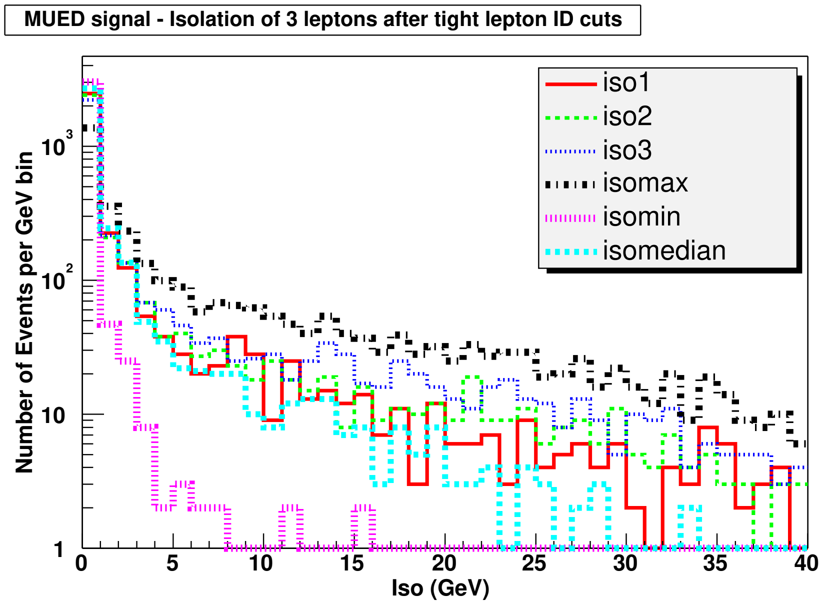

Figure 22: MUED signal MC isolation of three leptons after tight lepton cuts (as described in section 3.3). Isolation is defined as the energy in a cone of $\Delta R \equiv \sqrt{\Delta\phi^2 + \Delta\eta^2} = 0.4$ minus the electron or muon energy. iso1, iso2, iso3 are the isolations of the three leptons from the highest to the lowest transverse momentum respectively. isomax, isomin and isomedian are the maximum, minimum and median of the three isolations respectively.

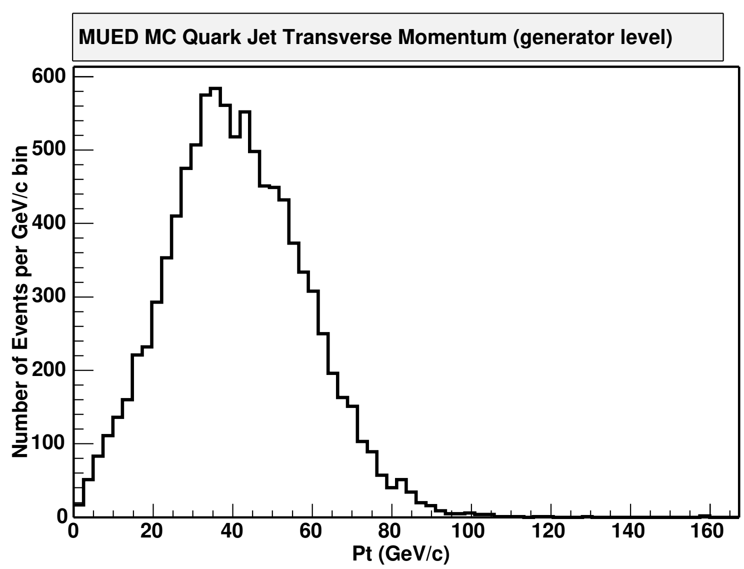

Figure 23: MUED signal MC transverse momentum of the quark jets from decays of SU(2)-doublet KK quarks.

D Run 1B Standard Model Background

The SUSY working group has generated a large background Monte Carlo samples for Run 1b analysis with ISAJET version 7_06 and 7_20. Files with two digit run-numbers are generated with version 7_06 using parton distribution function CTEQ-2L, MRSD0', and GRV-LO, and files with three digit run-numbers are generated with version 7_20 using parton distribution function CTEQ-3L and GRV-94LO.

Some of the samples have a selection applied on generator level. For the $b\bar{b}$, $c\bar{c}$ samples at least one b or c quark with $p_T > 10$ GeV/c in $|y| < 4.0$ [28] was required. The $b\bar{b}$, $c\bar{c}$, and Drell-Yan samples are required to have at least one high-p_T lepton ($p_T > 9.0$ GeV/c and $|\eta| < 1.5$) or two low-pT leptons ($p_T > 2.8$ GeV/c and $|\eta| < 3.0$). (Lepton stands for electron or muon.)

The production of $b\bar{b}/c\bar{c}$ MC sample was split up into 3 generation processes: direct three lepton production, initial state gluon radiation (ISR) and final state gluon radiation (FSR). Each of these processes was again split up in three areas according to the exchanged momentum with p_T ranging from 10 to 500 GeV/c. The nine data sets were each generated as a separate run. For each of the runs the event generation was performed with at least three different parton distribution functions.

The production of Drell-Yan was split up into 3 processes according to the exchanged particle: γ events with p_T ranging from 5 to 500 GeV/c; Drell-Yan Z^0 events with p_T ranging from 0.1 to 5 GeV/c and 5 to 500 GeV/c.

The production of $t\bar{t}$ events was generated with a p_T range of 0.1 to 500 GeV/c.

The production of Diboson W^+W^-, Z^0Z^0 and $W^\pm Z^0$ events was generated with a p_T range of 0.1 to 500 GeV/c.

Table 14,15,16,17 give details on the event generation.

[28] y denotes rapidity. The definition is $y = 0.5 ln\frac{E+P_z}{E-P_z}$. The shape of the rapidity distribution is invariant under a Lorentz boosts along the z-axis.

Table 14: SM $b\bar{b}/c\bar{c}$ background M.C. used in our analysis

Run Number	Type of Production	q range [GeV]	Structure Function	file sequence	lumi [pb^{-1}]	production tape
81	direct	[10, 25]	CTEQ2L	ka-kt	62.7	RK7442
			MRSD0'	la-lt	53.3	RK7625
			GRV_LO	ma-mt	59.1	RK7626
82	direct	[25, 50]	CTEQ2L	ka-kt	88.1	RK7628
						RK7872
			MRSD0'	la-lt	76.0	RK7865
						RK7872
			GRV_LO	ma-mt	98.3	RK7867
						RK7872
082			CTEQ3L	qa-qt	85.9	RK8364
						RK8367
			GRV_94	ra-rt	94.4	RK8463
						RK8465
83	direct	[50,500]	CTEQ2L	kp-kt	133.4	RK7874
			MRSD0'	la-lj	248.9	RK7872
			GRV_LO	ma-mj	336.7	RK7874
083			CTEQ3L	qa-qj	282.1	RK8367
						RK8369
84	ISR	[10, 25]	CTEQ2L	ka-kt	133.5	RK7634
			MRSD0'	la-lj	94.9	RK7934
			GRV_LO	ma-mj	58.2	RK7934
85	ISR	[25, 50]	CTEQ2L	ka-kt	132.9	RK7936
						RK7937
			MRSD0'	la-lt	157.3	RK7937
						RK7938
			GRV_LO	ma-mt	145.4	RK7938
						RK7939
085			CTEQ3L	qa-qt	145.6	RK8363
						RK8364
86	ISR	[50,500]	CTEQ2L	ka-kj	304.9	RK7940
			MRSD0'	la-lj	382.5	RK7940
						RK8003
			GRV_LO	ma-mj	387.9	RK8003
						RK8005
086			CTEQ3L	qj-qt	427.5	RK8370
87	FSR	[15, 25]	CTEQ2L	ka-ke	104.2	RK8005
			MRSD0'	la-le	92.5	RK8005
			GRV_LO	ma-md	89.8	RK8005
88	FSR	[25, 50]	CTEQ2L	ka-kt	60.5	RK8008
						RK8010
			MRSD0'	la-lt	54.4	RK8010
						RK8086
			GRV_LO	ma-mt	70.8	RK8086
						RK8087
088			CTEQ3L	qa-qt	167.4	RK8370
						RK8371
			GRV_94	ra-rt	192.8	RK8465
						RK8467
89	FSR	[50,500]	CTEQ2L	ka-kt	110.2	RK8087
						RK8089
						RK8090
			MRSD0'	la-lt	105.9	RK8090
						RK8094
			GRV_LO	ma-mt	142.0	RK8094
						RK8095
			CTEQ2L	na-nt	109.4	RK8266
						RK8267
			MRSD0'	oa-ot	105.5	RK8267
						RK8269
			GRV_LO	pa-pt	141.7	RK8273
						RK8363
089			CTEQ3L	qa-qt	321.3	RK8372
						RK8462
			GRV_94	ra-rt	389.9	RK8467
						RK8471

Table 15: SM Drell-Yan background M.C. used in our analysis

Run Number	**Exchanged Particle**	**q range [GeV]**	**Structure Function**	**file sequence**	**lumi** $[pb^{-1}]$	**production tape**
92	gamma	m=[5,500] t=[5,500]	CTEQ2L	ka-kt	483.7	RK7629
			MRSD0'	la-lt	431.8	RK7866
			GRV_LO	ma-mt	501.7	RK7868
092			CTEQ3L	qa-qj	241.3	RK8471
						RK8549
			GRV_94	ra-rj	254.8	RKB836
93	Z	m=[5,500] t=[5,500]	CTEQ2L	ka-kt	424.8	RK7869
			MRSD0'	la-lt	403.7	RK7871
			GRV_LO	ma-mt	446.3	RK7873
94	Z	m=[5,500] t=[0.1,5]	CTEQ2L	ka-kj	195.5	RKB840
			MRSD0'	la-lj	176.0	RKB841
			GRV_LO	ma-mj	217.3	RK7932

Table 16: SM $t\bar{t}$ background M.C. used in our analysis

Run Number	**q range [GeV]**	**Structure Function**	**file sequence**	**lumi** $[pb^{-1}]$	**production tape**
90	[0.1,500] m=175	CTEQ2L	ka-ke	5316.0	RK7627
		MRSD0'	la-le	5538.0	RK7627
		GRV_LO	ma-me	5558.0	RK7939
090		CTEQ3L	qa-qe	5430.0	RK8462
91	[0.1,500] m=175 noGLr	CTEQ3L	qa-qe	5466.0	RK9820

Table 17: SM boson pair background M.C. used in our analysis

Run Number	**Diboson Particle**	**q range [GeV]**	**Structure Function**	**file sequence**	**lumi** $[pb^{-1}]$	**production tape**
95	WW	[0.1,500]	CTEQ2L	ka-kc	2343.0	RKB843
			MRSD0'	la-lc	2154.0	RK7932
			GRV_LO	ma-mc	2373.0	RK7932
96	WZ	[0.1,500]	CTEQ2L	ka	5819.0	RK7932
			MRSD0'	la	5169.0	RK7932
			GRV_LO	ma	5696.0	RK7932
97	ZZ	[0.1,500]	CTEQ2L	ka	6843.0	RK7627
			MRSD0'	la	6590.0	RK8005
			GRV_LO	ma	7149.0	RK8269

E MUED Signal Monte Carlo Pythia TCL File

```
set useRCP t
mod input GenInputManager
mod enable Pythia

talk Pythia
PythiaMenu
cmEnergy set 1800
msel set 0
commonMenu

set_ckin -index=1 -value=900.
set_ckin -index=9 -value=-2
set_ckin -index=10 -value=2
set_ckin -index=11 -value=-2
set_ckin -index=12 -value=2

set_pmas -masscode=7 -mass=417.7 -width=2. -maxdev=20.
set_pmas -masscode=32 -mass=379.2 -width=2. -maxdev=20.
set_pmas -masscode=34 -mass=379.1 -width=2. -maxdev=20.
set_pmas -masscode=4000011 -mass=359.7 -width=2. -maxdev=20.
set_pmas -masscode=4000012 -mass=359.7 -width=2. -maxdev=20.
set_pmas -masscode=16 -mass=350.3

set_kfdp -channelIndex=65 -products=32,5
set_brat -channelIndex=65 -brRatio=0.2
set_mdme -channelIndex=65 -decayType=1 -matrix=0
set_kfdp -channelIndex=64 -products=-34,4
set_brat -channelIndex=64 -brRatio=0.8
set_mdme -channelIndex=64 -decayType=1 -matrix=0

set_mdme -channelIndex=56 -decayType=-1
set_mdme -channelIndex=57 -decayType=-1
set_mdme -channelIndex=58 -decayType=-1
set_mdme -channelIndex=59 -decayType=-1
set_mdme -channelIndex=60 -decayType=-1
set_mdme -channelIndex=61 -decayType=-1
set_mdme -channelIndex=62 -decayType=-1
```

```
set_mdme -channelIndex=63 -decayType=-1

set_kfdp -channelIndex=301 -products=13,-4000011
set_brat -channelIndex=301 -brRatio=0.25
set_mdme -channelIndex=301 -decayType=1 -matrix=0
set_kfdp -channelIndex=299 -products=-13,4000011
set_brat -channelIndex=299 -brRatio=0.25
set_mdme -channelIndex=299 -decayType=1 -matrix=0
set_kfdp -channelIndex=297 -products=11,-4000011
set_brat -channelIndex=297 -brRatio=0.25
set_mdme -channelIndex=297 -decayType=1 -matrix=0
set_kfdp -channelIndex=303 -products=-11,4000011
set_brat -channelIndex=303 -brRatio=0.25
set_mdme -channelIndex=303 -decayType=1 -matrix=0

set_mdme -channelIndex=289 -decayType=-1
set_mdme -channelIndex=290 -decayType=-1
set_mdme -channelIndex=291 -decayType=-1
set_mdme -channelIndex=292 -decayType=-1
set_mdme -channelIndex=293 -decayType=-1
set_mdme -channelIndex=294 -decayType=-1
set_mdme -channelIndex=295 -decayType=-1
set_mdme -channelIndex=296 -decayType=-1
set_mdme -channelIndex=298 -decayType=-1
set_mdme -channelIndex=300 -decayType=-1
set_mdme -channelIndex=302 -decayType=-1
set_mdme -channelIndex=304 -decayType=-1
set_mdme -channelIndex=305 -decayType=-1
set_mdme -channelIndex=306 -decayType=-1
set_mdme -channelIndex=307 -decayType=-1
set_mdme -channelIndex=308 -decayType=-1
set_mdme -channelIndex=309 -decayType=-1
set_mdme -channelIndex=310 -decayType=-1

set_kfdp -channelIndex=330 -products=-13,-4000012
set_brat -channelIndex=330 -brRatio=0.25
set_mdme -channelIndex=330 -decayType=1 -matrix=0
set_kfdp -channelIndex=329 -products=-11,-4000012
set_brat -channelIndex=329 -brRatio=0.25
set_mdme -channelIndex=329 -decayType=1 -matrix=0
set_kfdp -channelIndex=328 -products=-4000011,-14
```

set_brat -channelIndex=328 -brRatio=0.25
set_mdme -channelIndex=328 -decayType=1 -matrix=0
set_kfdp -channelIndex=327 -products=-4000011,-12
set_brat -channelIndex=327 -brRatio=0.25
set_mdme -channelIndex=327 -decayType=1 -matrix=0

set_mdme -channelIndex=311 -decayType=-1
set_mdme -channelIndex=312 -decayType=-1
set_mdme -channelIndex=313 -decayType=-1
set_mdme -channelIndex=314 -decayType=-1
set_mdme -channelIndex=315 -decayType=-1
set_mdme -channelIndex=316 -decayType=-1
set_mdme -channelIndex=317 -decayType=-1
set_mdme -channelIndex=318 -decayType=-1
set_mdme -channelIndex=319 -decayType=-1
set_mdme -channelIndex=320 -decayType=-1
set_mdme -channelIndex=321 -decayType=-1
set_mdme -channelIndex=322 -decayType=-1
set_mdme -channelIndex=323 -decayType=-1
set_mdme -channelIndex=324 -decayType=-1
set_mdme -channelIndex=325 -decayType=-1
set_mdme -channelIndex=326 -decayType=-1
set_mdme -channelIndex=331 -decayType=-1
set_mdme -channelIndex=332 -decayType=-1
set_mdme -channelIndex=333 -decayType=-1
set_brat -channelIndex=311 -brRatio=0
set_brat -channelIndex=312 -brRatio=0
set_brat -channelIndex=313 -brRatio=0
set_brat -channelIndex=314 -brRatio=0
set_brat -channelIndex=315 -brRatio=0
set_brat -channelIndex=316 -brRatio=0
set_brat -channelIndex=317 -brRatio=0
set_brat -channelIndex=318 -brRatio=0
set_brat -channelIndex=319 -brRatio=0
set_brat -channelIndex=320 -brRatio=0
set_brat -channelIndex=321 -brRatio=0
set_brat -channelIndex=322 -brRatio=0
set_brat -channelIndex=323 -brRatio=0
set_brat -channelIndex=324 -brRatio=0
set_brat -channelIndex=325 -brRatio=0
set_brat -channelIndex=326 -brRatio=0
set_brat -channelIndex=331 -brRatio=0

```
set_brat -channelIndex=332 -brRatio=0
set_brat -channelIndex=333 -brRatio=0

set_kfdp -channelIndex=3858 -products=11,16
set_brat -channelIndex=3858 -brRatio=0.5
set_mdme -channelIndex=3858 -decayType=1 -matrix=0
set_kfdp -channelIndex=3859 -products=13,16
set_brat -channelIndex=3859 -brRatio=0.5
set_mdme -channelIndex=3859 -decayType=1 -matrix=0
set_mdme -channelIndex=3857 -decayType=-1

set_kfdp -channelIndex=3860 -products=14,16
set_brat -channelIndex=3860 -brRatio=0.5
set_mdme -channelIndex=3860 -decayType=1 -matrix=0
set_kfdp -channelIndex=3861 -products=12,16
set_brat -channelIndex=3861 -brRatio=0.5
set_mdme -channelIndex=3861 -decayType=1 -matrix=0

set_mstp -index=7 -value=7
set_msub -index=81 -value=1
set_msub -index=82 -value=1

exit
exit
exit

talk Pythia
PythiaMenu
statListLevel set 2
commonMenu
show_mdcy
show_kfdp
show_mdme
show_brat
exit
exit
exit

talk FileOutput
```

```
output create main_stream b1pair_350_10.sim
output path main_stream AllPath
output keepList main_stream
LRID_StorableBank LRIH_StorableBank EVCL_StorableBank
HEPG_StorableBank OBSP_StorableBank OBSV_StorableBank
exit

begin -nev 10000
show timer

exit
```

F $b\bar{b}/c\bar{c}$ Background Scale Factor

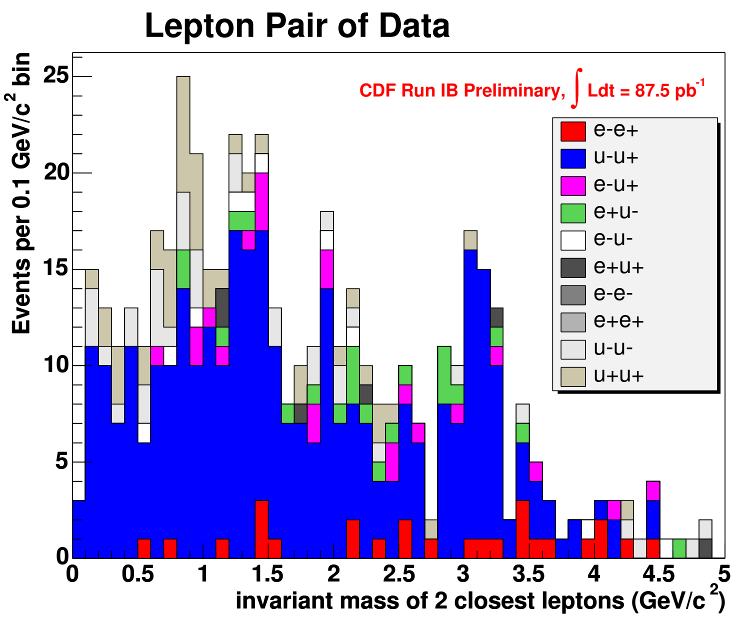

Figure 24: Data invariant mass of the two closest leptons in the less than 5 GeV region by lepton pair type.

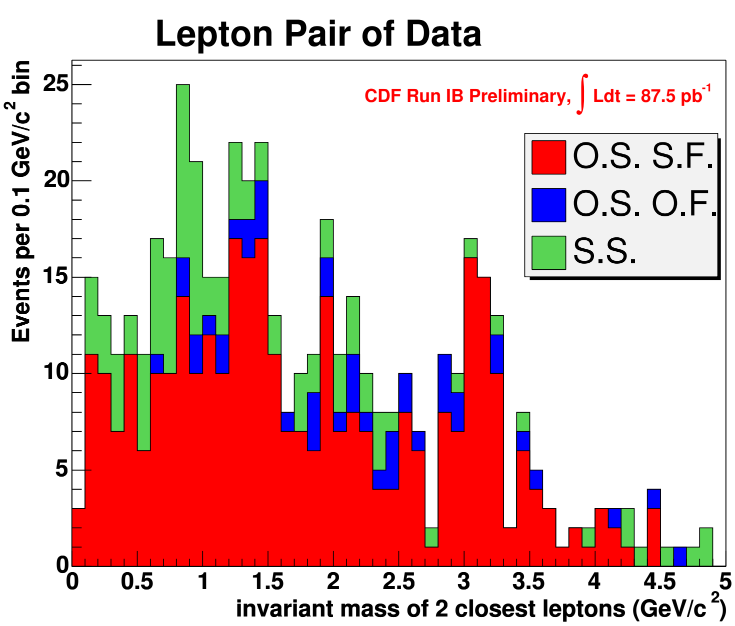

Figure 25: Data invariant mass of the two closest leptons in the less than 5 GeV region by lepton pair type.

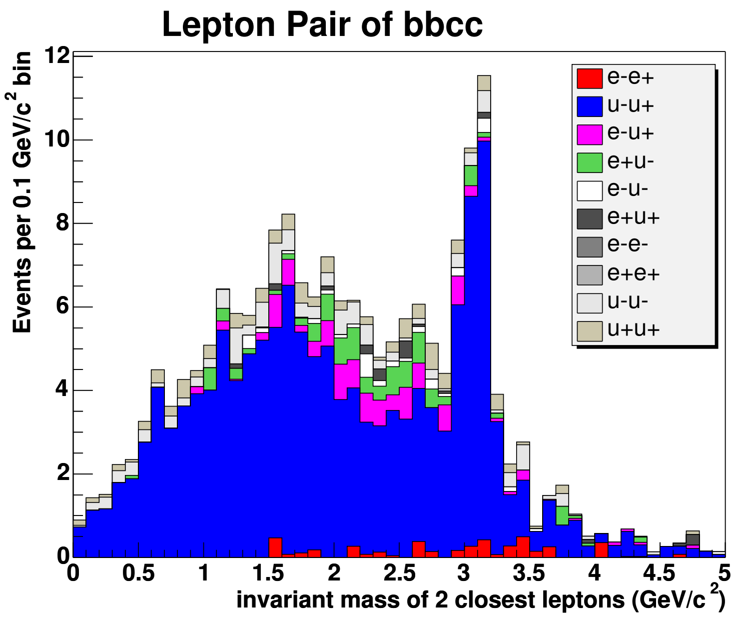

Figure 26: bbcc invariant mass of the two closest leptons in the less than 5 GeV region by lepton pair type.

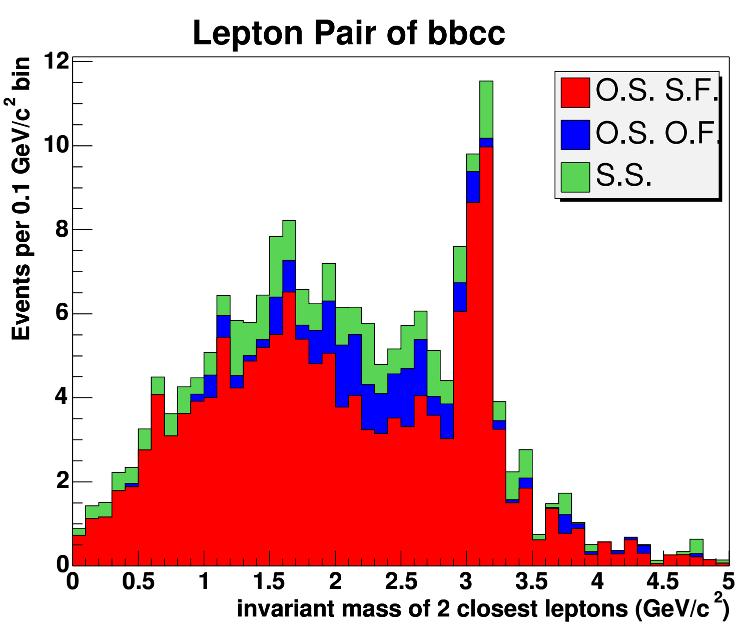

Figure 27: bbcc invariant mass of the two closest leptons in the less than 5 GeV region by lepton pair type.

We examined the invariant mass of the two closest leptons in the less than 5 GeV region by their lepton pair types, see Figure 24,25,26,27.

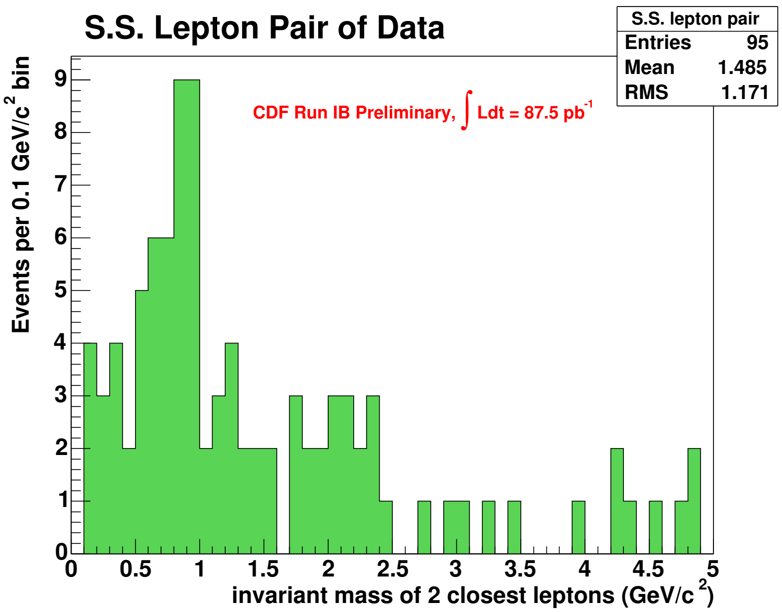

Figure 28: Data invariant mass of the two closest leptons in the less than 5 GeV region same sign lepton pair.

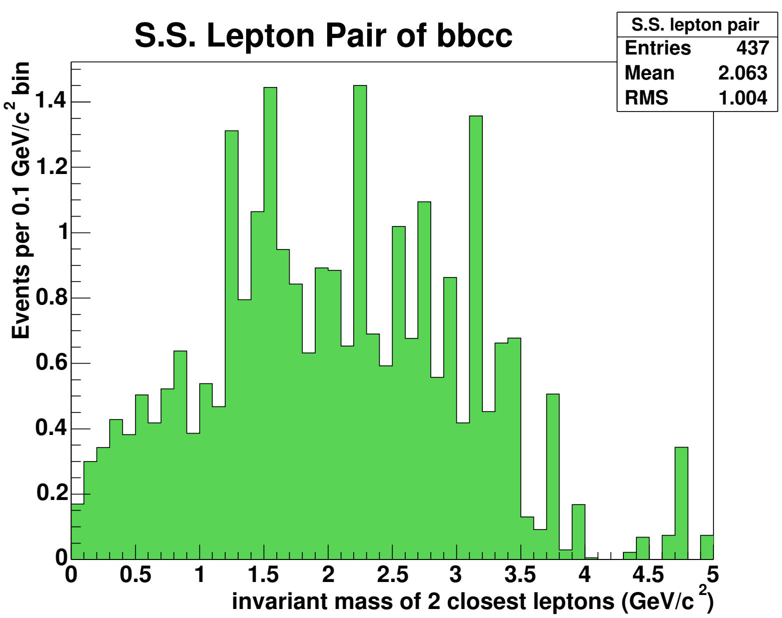

Figure 29: bbcc invariant mass of the two closest leptons in the less than 5 GeV region same sign lepton pair.

For a closer look at the same sign lepton pair invariant mass, see Figure 28,29.

Our conclusion is:

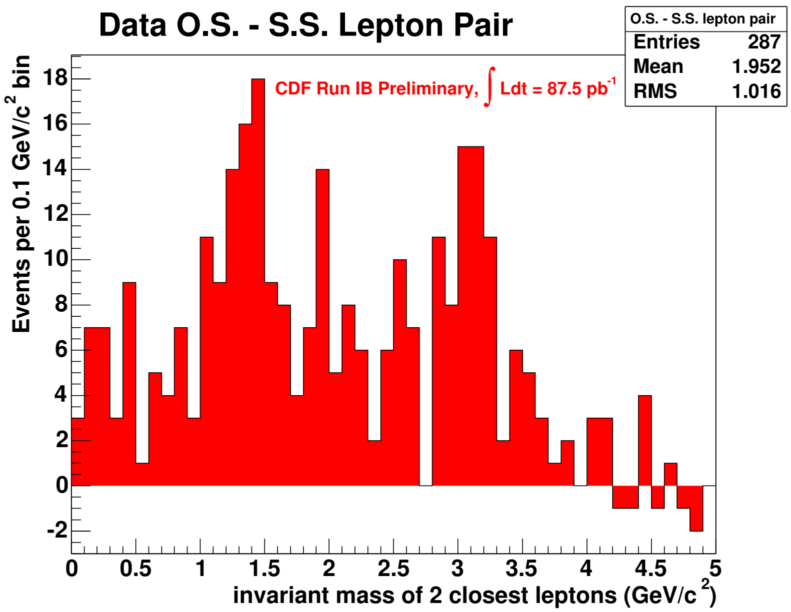

Figure 30: Data invariant mass of the two closest leptons in the less than 5 GeV region opposite sign lepton pair subtract same sign lepton pair.

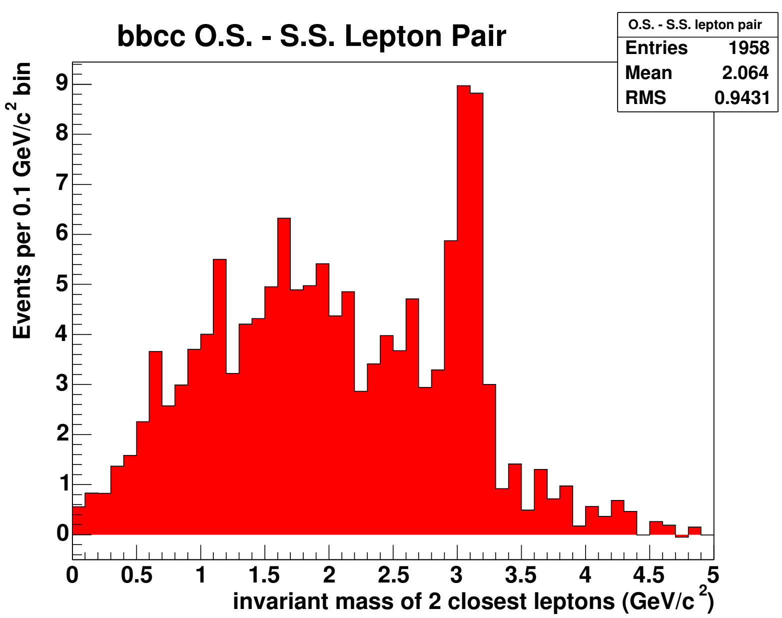

Figure 31: bbcc invariant mass of the two closest leptons in the less than 5 GeV region opposite sign lepton pair subtract same sign lepton pair.

1. J/psi estimation from other sources is not significant. There are even less J/psi's in data than bbcc generated.

2. There are significant number of fakes from same sign (S.S.) lepton pairs in data, especially the low invariant mass region. These SS events in the data look nothing like real bb, and that we expect them to be dominated by fakes, which are roughly sign-symmetric.

3. The exact invariant mass distribution from bbcc depends upon getting not just the inclusive muon and electron branching ratios correct, but the particular exclusive decay modes as well. This is why we'd rather take all data below 5 GeV, rather than cutting on a particular value - that we expect the integral to be correct, while the exact shape may be a little off.

Our approach is to subtract the effect of SS lepton pairs from OS lepton pairs, and do the bbcc scaling in the 0 to 5 GeV region. There are a small amount SS lepton pairs from bbcc as well, presumably generated in the bbcc simulation, however they should be subtracted as well because they may not be simulated correctly.

Invariant mass plot with SS lepton pairs subtracted from OS lepton pairs, see Figure 30,31.

The bbcc scale factor is 287/137.546 = 2.1 (2.08657)

Root Kolmogorov test of the shape between bbcc and data result is 0.254 (the value is the compatibility probability of test), so they are somewhat compatible.

Notes:

We removed events if there is a PEM electron in one of the two closest leptons because the charge sign of PEM cannot be determined. There are 0 out of 477 events in data, and 6 out of 2838 events in bbcc.

Table 18: Number of data and $b\bar{b}/c\bar{c}$ events in each channel, invariant mass of 2 closest lepton in less than 5 GeV region.

Lepton Pair	e^-e^+	$\mu^-\mu^+$	$e^-\mu^+$	$e^+\mu^-$	$e^-\mu^-$	$e^+\mu^+$	e^-e^-	e^+e^+	$\mu^-\mu^-$	$\mu^+\mu^+$	Total
data	26	312	22	22	10	6	0	0	37	42	477
$b\bar{b}/c\bar{c}$	4.456	140.568	10.125	8.986	2.978	1.951	0	0	12.411	9.249	190.724

Table 19: Number of data and $b\bar{b}/c\bar{c}$ events in each channel, invariant mass of 2 closest leptons in less than 5 GeV region.

Channel	eee	$ee\mu$	$e\mu\mu$	$\mu\mu\mu$	Total
data	9	36	100	332	477
$b\bar{b}/c\bar{c}$	0.070	11.453	54.201	125.324	191.047

G Charged Multiplicity

The signature of the UED signal is multiple standard leptons, jets and missing energy. We do not use the jets signature in our event selection directly, - this is because the data sample we use has a relatively low integrated luminosity, and we can suppress most background events without requiring jets identification.

If we had a large amount of data (or perhaps for CDF Run II analysis), jets identification maybe required to further reduce background events. An alternative method is to include event charged multiplicity cut because jets activity will increase the event charged multiplicity.

We studied the effect of charged multiplicity [29] cut together with isolation cut and $\not{E}_T$ cut in the final cuts optimization.

We searched a cut matrix with isolation range from 2 GeV to 10 GeV with a step size of 1 GeV, $\not{E}_T$ range from 10 GeV to 30 GeV with a step size of 1 GeV, and charged multiplicity range from 0 to 10 with a step size of 1. In Fig. 32, we plot the optimization value $\mathbb{A}$, where $a = 95\%$, with each grid point and charged multiplicity value. We found the following cuts maximize $\mathbb{A}$ for all channels:

$$ISO < 6 \text{ GeV}, \ \not{E}_T > 20 \text{ GeV}, \ \text{Charged Multiplicity} > 6 \tag{28}$$

The number of events expected before and after the final optimization cuts are listed in Appendix H.

The separate cut optimization for the non-$\mu\mu\mu$ channels and the $\mu\mu\mu$ channel are shown in Fig. 33 and Fig. 34

We found the following cuts maximize $\mathbb{A}$ for the non-$\mu\mu\mu$ channels:

$$ISO < 4 \text{ GeV}, \ \not{E}_T > 15 \text{ GeV}, \ \text{Charged Multiplicity} > 6 \tag{29}$$

and the following cuts maximize $\mathbb{A}$ for the $\mu\mu\mu$ channels:

$$ISO < 8 \text{ GeV}, \ \not{E}_T > 20 \text{ GeV}, \ \text{Charged Multiplicity} > 6 \tag{30}$$

Fig. 35 shows the charged multiplicity distribution of the MUED signal Monte Carlo, the SM background, and data, before imposing the final optimization cuts, in the non-$\mu\mu\mu$ channels.

[29] We calculate the event charged multiplicity by counting the number of charged tracks with $p_T > 2\ GeV/c$. We studied counting with various p_T requirements and 2 GeV/c has the best separation power.

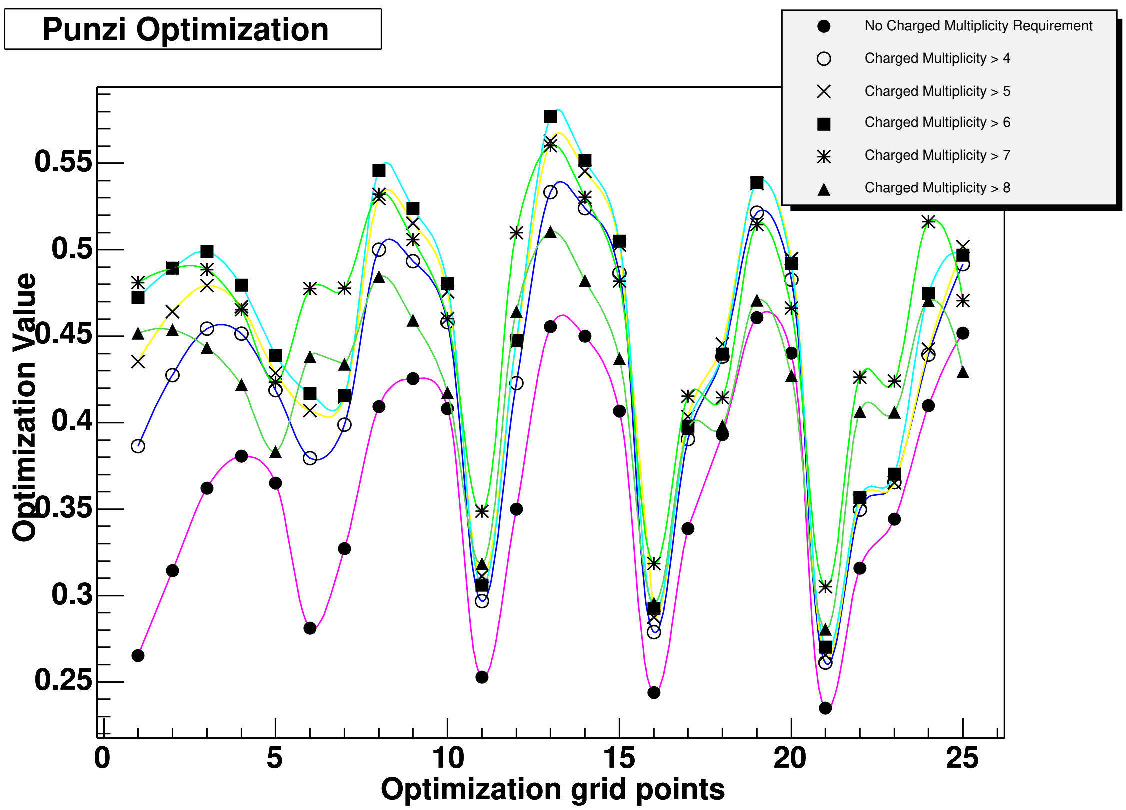

Figure 32: Punzi search of the cut matrix to optimize value $\mathbb{A}$ (y axis), with $a = 95\%$. See Table. 11 for (x axis) grid points.

Table 20 lists the number of events expected before and after the final optimization cuts from each type of background, the sum of all background, the number of data events and a sample MC signal point, separated into non-$\mu\mu\mu$ channels and $\mu\mu\mu$ channel.

We decide not to use charge multiplicity cut because it doesn't improve our result [30]. In the non-$\mu\mu\mu$ channels before charged multiplicity cut there are 0.05 background, after charged multiplicity cut there are 0.02 background [31]. In addition, using charged multiplicity cut will increase the systematic uncertainty [32]. Furthermore, without charged multiplicity cut, the total detection efficiency can be improved so we can obtain better cross section limit (see Table 21).

[30] Note that the optimal Punzi cuts for isolation and $\not\!\!E_T$ are the same whether we use the charged multiplicity cut or not, see Fig. 32,33,34.

[31] The number of expected events is the same 3.08 events in both cases using Bayesian method

[32] [30] studies quark and gluon jet charged track multiplicities and compares the Herwig and Pythia MC samples with the data. It indicates that for a 40 GeV jet with p_T cut of 500 MeV/c there are 30% systematic uncertainties of quark jets track multiplicities. Even though we use event charged multiplicity instead of jet charged multiplicity, and our p_T cut is at 2 GeV/c instead of 500 MeV/c, a systematic uncertainty still need to be assigned if we use charged multiplicity cut.

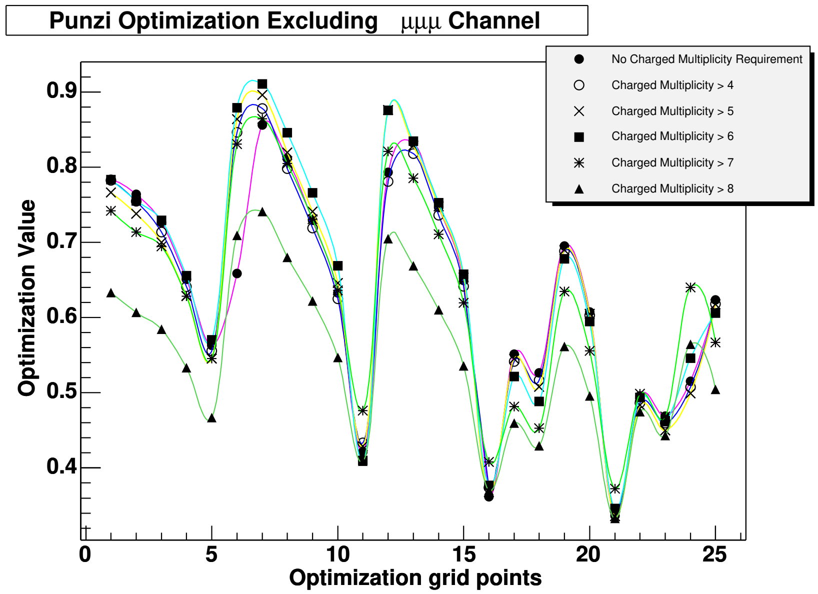

Figure 33: Punzi search in non-$\mu\mu\mu$ channel of the cut matrix to optimize value $\mathbb{A}$ (y axis), with $a = 95\%$. See Table. 11 for (x axis) grid points.

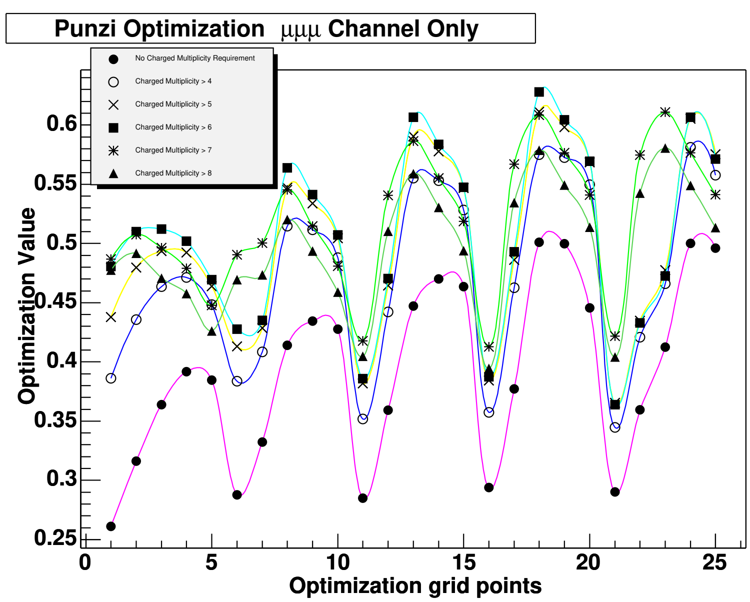

Figure 34: Punzi search in $\mu\mu\mu$ channel of the cut matrix to optimize value $\mathbb{A}$ (y axis), with $a = 95\%$. See Table. 11 for (x axis) grid points.

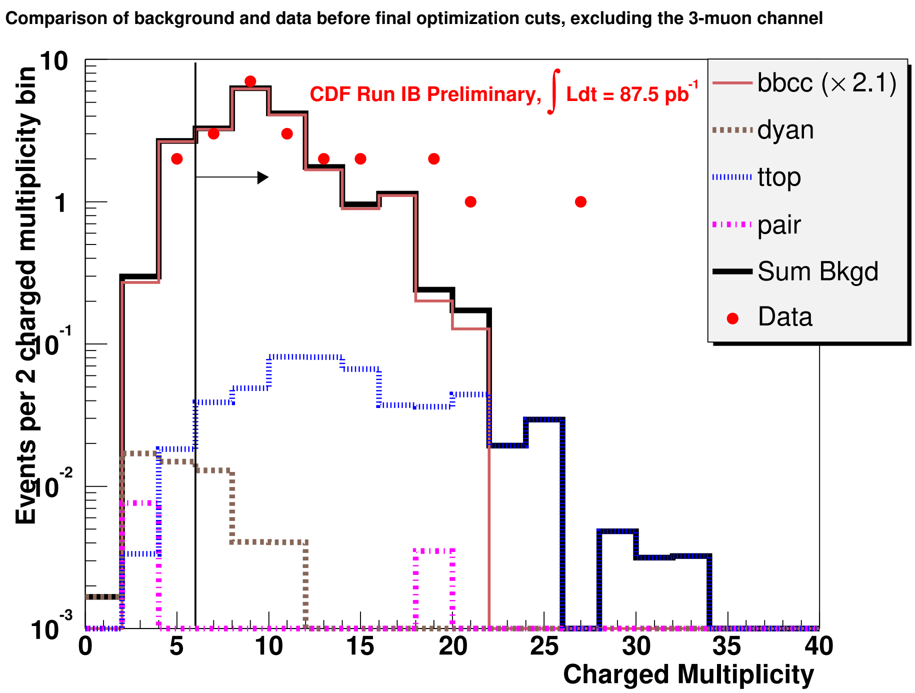

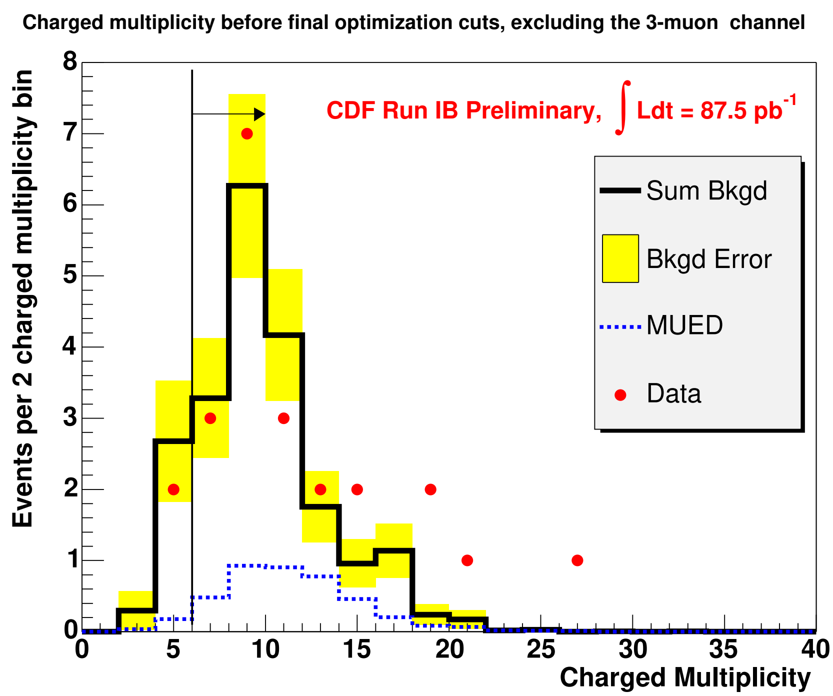

Figure 35: Distributions of charged multiplicity in the non-$\mu\mu\mu$ channels. The top figure shows data and each type of background. The bottom figures shows the MUED signal, data and the total background with error band. The scale factor 2.1 is applied to $b\bar{b}/c\bar{c}$ background, and the total background includes $b\bar{b}/c\bar{c}$ background with scale factor 2.1 applied, Drell-Yan, $t\bar{t}$, and boson pairs. The vertical straight lines indicate the cut value and the arrows indicate the accepted values. Background MC samples are generated by SUSY working group (Appendix D).

Table 20: Separated into non-$\mu\mu\mu$ channels and $\mu\mu\mu$ channel, number of expected background events contributed by $b\bar{b}/c\bar{c}$, Drell-Yan, $t\bar{t}$ and boson pair production, total number of expected background, data and signal Monte Carlo events remaining after each cut. All MC events are properly weighted with luminosity, lepton ID efficiency, and trigger efficiency.

	Events remaining after each cut						
non-$\mu\mu\mu$ channels	$b\bar{b}/c\bar{c}$	Drell-Yan	$t\bar{t}$	Boson Pair	Sum Background	Data	Signal MC ($R^{-1} = 350\ GeV$)
before final optimization cuts	20.43	0.06	0.52	0.01	21.02	23	0.64
$ISO < 4$ GeV	0.44	0.04	0.04	0.00	0.52	3	0.42
$\not{E}_T >$ 15 GeV	0.00	0.01	0.04	0.00	0.05	0	0.38
Charged Multiplicity > 6	0.00	0.00	0.01	0.00	0.02	0	0.34

	Events remaining after each cut						
$\mu\mu\mu$ channel	$b\bar{b}/c\bar{c}$	Drell-Yan	$t\bar{t}$	Boson Pair	Sum Background	Data	Signal MC ($R^{-1} = 350\ GeV$)
before final optimization cuts	17.70	4.81	0.44	0.04	22.99	20	0.26
$ISO < 8$ GeV	1.87	4.71	0.05	0.01	6.64	14	0.20
$\not{E}_T >$ 20 GeV	0.00	0.71	0.05	0.00	0.76	1	0.16
Charged Multiplicity > 6	0.00	0.17	0.04	0.00	0.21	1	0.16

Table 21: Total Detection Efficiency (non-$\mu\mu\mu$, $\mu\mu\mu$)

Sample	with charged multiplicity	without charged multiplicity
Q_1Q_1	4.6% (3.2%, 1.4%)	5.0% (3.5%, 1.5%)
g_1Q_1	3.0% (2.1%, 0.9%)	3.0% (2.1%, 0.9%)
g_1g_1	3.0% (2.0%, 1.0%)	3.0% (2.0%, 1.0%)

H Expected Backgrounds before and after the Final Optimization Cuts in All Channels

Table 22 lists the number of events expected before and after the final optimization cuts from each type of background, the sum of all background, the number of data events and a sample MC signal point in all channels.

Table 22: In all channels, number of expected background events contributed by $b\bar{b}/c\bar{c}$, Drell-Yan, $t\bar{t}$ and boson pair production, total number of expected background, data and signal Monte Carlo events remaining after each cut. All MC events are properly weighted with luminosity, lepton ID efficiency, and trigger efficiency.

	Events remaining after each cut						
all channels	$b\bar{b}/c\bar{c}$	Drell-Yan	$t\bar{t}$	Boson Pair	Sum Background	Data	Signal MC ($R^{-1} = 350\ GeV$)
before final optimization cuts	38.14	4.87	0.96	0.05	44.02	43	0.90
$ISO < 6$ GeV	3.93	4.74	0.10	0.02	8.79	15	0.64
$\not{E}_T > 20$ GeV	0.00	0.71	0.09	0.00	0.80	1	0.54
Charged Multiplicity > 6	0.00	0.17	0.06	0.00	0.23	1	0.50

I Event Display: Run 63604 Event 108434

There is one event left after all cuts in the $\mu\mu\mu$ channel. The event displays are shown in Figure 36 and 37.

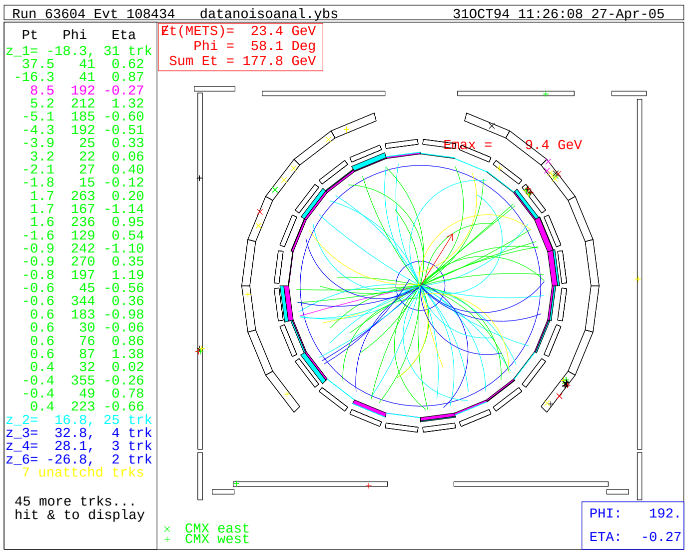

Figure 36: Event:Run 63604 Event 108434

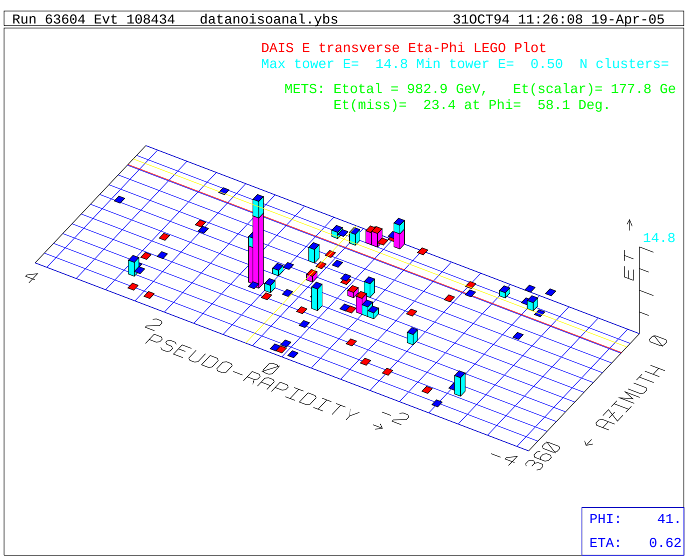

Figure 37: Event:Run 63604 Event 108434

The three lepton candidates are central muon, extension muon and central muon, sorted by transverse momentum in the descending order. Table 23 shows the kinematics of the event.

The invariant mass of the two closest leptons is 5.45 GeV/c^2.
The missing energy of the event is 24.1 GeV.
There are 15 charged tracks with p_T greater than 2 GeV/c.

Table 23: Three Lepton Candidates of Event:Run 63604 Event 108434

	1st lepton	2nd lepton	3rd lepton
Species	CMU/P	CMX	CMU/P
p_T(GeV/c)	30.45	-15.71	8.98
ϕ (Radian)	0.71	0.71	3.35
η	0.62	0.87	-0.27
Isolation (GeV)	2.65	2.49	3.30